INVESTIGATION OF THE PATHOLOGY OF BRAIN DERIVED ENDOTHELIAL CELLS IN *IN-VITRO* HYPOXIA MODELS

A Thesis Submitted to
The Graduate School of Engineering and Sciences of
İzmir Institute of Technology
in Partial Fulfillment of the Requirements for the Degree of

MASTER OF SCIENCE

in Molecular Biology and Genetics

by
Kısmet Tuğçe ERDEMLİ

July 2021
İZMİR

ACKNOWLEDGMENTS

I wish to express my sincerely thanks to my supervisor Assist. Prof. Dr. Çiğdem TOSUN for her guidance, encouragement, and endless support. She has always been kind to me and she did best for me to improve my scientific knowledge. I will be always grateful for allowing me to join her lab.

I deeply thank to my committee members Prof. Dr. Hüseyin Çağlar KARAKAYA and Assoc. Prof. Dr. Duygu SAĞ WİNGENDER for their contributions and support.

I also would like to thank Assoc. Prof. Dr. Gülistan MEŞE ÖZÇİVİCİ who allow me to use fluorescent microscope, and her student Yağmur Ceren ÜNAL who helped me and answered my all questions, Assoc. Prof. Dr. Alper ARSLANOĞLU who let me to use hood for cell culture experiments and also Prof.Dr. Petek BALLAR KIRMIZIBAYRAK who allow me to done my Western blot experiments, and her student Recep İLHAN who explain everything.

I would like to thank my friends Ece YAZICI who always there for me, Ahmet Salih ÜNAL who is my friend forever, Mustafa ERDOĞMUŞ, Yasemin BİLGİ, S. Merve ÖZDEMİR, and Gizem Tuğçe ULU. They are lovely friends and support me all times when I struggled problems.

I offer my deepest gratitude to my lovely family, Gülçin ERDEMLİ, Emin ERDEMLİ, and Buse Nur ERDEMLİ for their endless love and support. They have always believed and motivated me throughout my life. I will be always grateful for them and always love them.

ABSTRACT

INVESTIGATION OF THE PATHOLOGY OF BRAIN DERIVED ENDOTHELIAL CELLS IN *IN-VITRO* HYPOXIA MODELS

The blood brain barrier (BBB) is a vital structure that protects brain homeostasis. Endothelial cells (EC) have a significant role in regulating the BBB structure and function. Several studies have revealed the association of SUR1-TRPM4 channels that regulate this secondary damage of CNS injuries. After the activation of the channel, Na^+ influx causes depolarization, cell swelling (edema) and ultimately oncotic cell death. Hypoxia inducing factor (HIF) transcription factor that has been reported to activate more than 100 genes to adapt to a hypoxic condition. Once Hif1-α is translocated into the nucleus, it can dimerize with HIF1-ß to produce HIF that is critical in hypoxic conditions and regulate cell cycle arrest or cell death pathways. Hypoxia can occur in an O_2 dependent and independent manner. In this study, $CoCl_2$ and hypoxia chamber which was cost-effective and reliable were optimized.

Cellular death was calculated with Trypan blue staining in this novel hypoxia chamber model and compared with $CoCl_2$ models. In addition, morphological changes were observed in microscopic analysis. Hif1-α, caspase-3 and NF-κB translocation to the nucleus localization were quantified. Cell viability was different between the $CoCl_2$ model and novel hypoxia chamber model at 24 hours. The cellular death increased with $CoCl_2$ exposure, where no change was noted in the hypoxia chamber model. Time dependent Hif1-α upregulation was also demonstrated that peaked at 12-hours. Finally, NF-κB translocation into the nucleus was significantly increased at 24 hours of hypoxia exposure.

The results reveal that the inflatable hypoxia chamber model could be reliably used to mimic hypoxia in an *in-vitro* setting. Hif1-α activated in a time dependent manner, along with NF-κB. The upregulation of these transcription factors can ultimately affect the cellular death mechanisms differently.

ÖZET

BEYİN ENDOTEL HÜCRELERİ'NİN *İN-VİTRO* HİPOKSİ MODELLERİ İLE KARAKTERİZASYONUN İNCELENMESİ

Kan-beyin bariyeri (KBB), beyin homeostazını koruyan önemli bir yapıdır. KBB yapısını ve işlevini düzenlemede endotel hücreleri önemli bir role sahiptir. Birçok çalışma, merkezi sinir sistemi (MSS) yaralanmalarının, ikincil hasarı düzenleyen SUR1-TRPM4 kanalları ile ilişkisi olduğunu ortaya çıkarmıştır. Kanalın aktivasyonu ile Na^+ hücre içine geçer daha sonra ise, depolarizasyona, hücre şişmesine (ödem) ve onkotik hücre ölümüne sebep olur. Hipoksi indükleyici faktör 1 (HIF1), hücrelerde hipoksik ortama uyum sağlamak için 100'den fazla geni aktive eder. Hif1-α çekirdeğe geçtikten sonra HIF1-ß ile HIF1'ı oluşturur. HIF1 hipoksik koşullara uyum sağlamak ile görevli birçok farlı gen transkripsiyonunu düzenler. Bunlar, hücre döngüsünü düzenleyen genler ya da hücre ölümünü tetikleyen genler olabilir. HIF1 O_2 den bağımlı ya da bağımsız şekilde aktive edilebilir. Bu çalışmada, uygun maliyetli ve güvenilir hipoksi modeli ile birlikte $CoCl_2$ modeli optimize edilmiştir.

Hücre ölümü, yeni hipoksi modelinde ve $CoCl_2$ modelinde Tripan mavisi boyaması ile hesaplandı Ek olarak, mikroskobik analizde morfolojik değişiklikler gözlemlendi. Çekirdekteki Hif1-α, kaspaz-3 ve NF-κB translokasyonu analiz edildi. Hücre ölümü, 24-saat hipoksik ortama maruz kalmış $CoCl_2$ modeli ve yeni hipoksi modelinin sonuçları birbirinden farklıydı. Hipoksi modelinde hücre ölümünde hiçbir değişiklik olmazken, $CoCl_2$ modelinde hücre ölümü artmıştır. Zamana bağlı Hif1-α'nin çekirdekteki translokasyonu 12 saatte zirve yaptığı gözlemlenmiştir. Ayrıca, NF-κB'nin çekirdeğe translokasyonu, 24 saatlik hipoksik koşullarda önemli ölçüde arttı.

Sonuçlara göre yeni hipoksi modeli, *in-vitro* ortamda hipoksiyi taklit etmek için kullanılabilmektedir. Hif1-α, NF-κB ile birlikte zamana bağlı bir şekilde aktive edildi. Transkripsiyon faktörlerinin artması ya da azalması, hücresel ölüm mekanizmalarını farklı şekilde etkileyebilir.

TABLE OF CONTENT

LIST OF TABLES

LIST OF FIGURES

Figure **Page**

Figure **Page**

CHAPTER 1

INTRODUCTION

1.1. Blood-Brain Barrier

Blood spreads from the heart to all tissues via blood vessels to deliver nutrients and oxygen, remove carbon dioxide and metabolic wastes, transport signaling molecules to the body and regulate the immune system to protect the body (Daneman 2015). The central nervous system (CNS) is an enclosed system where neurons communicate with others via particular chemical and electrical signals. The microenvironment inside the CNS system is critical in maintaining brain homeostasis. For this reason, blood vessels in the CNS have a very particular structure that has been conserved throughout evolution, 1forming the blood-brain barrier (BBB). The BBB structure develops early in life of the fetus approximately 14 weeks of age and is fully completed with birth. The earlier form of the BBB protects brain tissue from macromolecules (Virgintino 2004). BBB regulates the passage of many different molecules, ions, and cells from the blood to the brain and vice versa. The regulation of molecules between BBB and blood has critical importance in protecting neuronal function and communication. BBB also keeps away toxins, pathogens, and inflammatory cells from CNS (Daneman 2015; Abbott 2006). The pH and some ions such as K^+, Ca^+, Mg^{+2} are regulated continuously at the BBB to supply a suitable environment for neurons. Blood contains some neurotransmitters such as glutamate, an amino acid essential in neuronal excitation. BBB does not pass these kinds of macromolecules to minimize the wrong neuronal activation. Some plasma proteins and neurotoxins can damage neuronal tissue; thus they need to be kept away from the CNS (Abbott 2010). On the other hand, oxygen, carbon dioxide, and small lipophilic molecules can pass through the BBB by diffusion. Glucose, amino acids, and nutrients required for brain tissue is transported by the help of carrier-mediated transporters. Larger molecules like insulin and leptin can pass with receptor-mediated endocytosis. Thus, the transport of substances needs to be tightly regulated by endothelial cells (EC) that are specialized for this function in the BBB (Kadry *et al.* 2010). Compared to other vascular endothelial

cells, microvascular endothelial cells have a unique morphology, structure, and function. Microvascular endothelial cells have tight junction proteins. Therefore, ECs limit the passage of polar molecules and require the need for additional energy-dependent transportation mechanisms. They also lack transcellular junctions and pinocytosis (Kadry *et al.* 2010). Even though endothelial cells are essential for the structure of the BBB, other cells are also necessary for the integrity of BBB, and regulation of molecular transport (Keaney *et al.* 2015). Accordingly, several cells surround the brain capillaries endothelial cells to form the neurovascular unit (NVU). The neurovascular unit helps to develop the BBB as a functional barrier. These helper cells are astrocytes, pericytes and neurons. NVU also contains a basement membrane (BM) to help regulate signal transduction. Pericytes surround the abluminal side of the brain capillaries with their extensions (Langen 2019). They are found inside the BM, localized between ECs and astrocytes. Pericytes have essential functions in maintaining BBB integrity by regulating specific gene expression in ECs and enhance microvascular stability as an astrocyte polarization inducer to produce astrocyte end-feet. They also serve in the transport of molecules between neurons and the vasculature (Armulik *et al.* 2010). Another cell type of the NVU is astrocytes that maintain the barrier function of the BBB. They have specialized astrocytic end-feet that enable them to form direct interactions with ECs. By this way, they act as a bridge between ECs and neurons to transport molecules. Astrocytes have a significant role in neuroinflammation. They contribute to form the BM by producing extracellular matrix (ECM) proteins. Astrocytes also regulate BBB integrity via signaling pathways. For example, apolipoprotein E released from astrocytes specifically binds to ECs or pericytes via low-density lipoprotein receptor (LRP1). The last component of the NVU of the basement membrane is the ECM that supports NVU cells and produce a suitable environment for proper communication. The ECM of the BM is composed of type IV collagen, fibronectin, laminin, and glycoproteins. The enzyme matrix metallopeptidase-9 (MMP-9) causes deficits in the BM by destroying cellular communication between NVU cells and the BBB integrity by degrading collagen (Lenglet et al. 2015). These cells and the communication among them provide a dynamic BBB structure that regulate permeability and transportation. Many chemicals secreted from the NVU cells or inside blood can affect transportation mechanisms and endothelial cell permeability (Tonra 2002). Histamine inside the blood or ATP from astrocytic neuronal firing mechanism can increase glucose uptake in neurons. Pericytes signal to astrocytes and their astrocytic end-feet. Astrocytic end-feet can regulate the transportation

between neurons and the vasculature. Overgrowth of astrocytic end-feet promotes an upregulation of transportation.

1.1.1. Brain microvascular endothelial cells (BMECs)

Brain microvascular endothelial cells (BMECs) are important structural barrier cells that maintain blood supply to the BBB. BMECs are highly specialized cells in their morphology and metabolic systems. They have elongated central nuclei (Yu *et al.* 2015). Their metabolic activity is high with an increased number of mitochondria to generate energy that is required for the transportation of molecules in and out of brain cells. They need many different molecular mechanisms to carry out transportation and to maintain brain homeostasis. Several specific ion channels, receptors, and transport proteins are required for the transport (Abdullahi *et al.* 2018). BMECs have specialized anatomical properties to protect brain homeostasis. They lack transcellular holes and pinocytic activity of ECs and have highly regulated adherent junctions (AJs) and tight junctions (TJs). TJs are formed between intercellular ECs to limit the diffusion of polar molecules and macromolecules between ECs (Lochhead 2020). TJs makes the impermeable barrier that is important in BBB integrity. This barrier function is evaluated by trans endothelial resistance (TEER) which is 1,500-2,000 ohm.cm2 for BMECs but, is 3-30 ohm.cm2 for peripheral endothelial cells. TEER value shows that BMECs' permeability is much lower than other endothelial cells. The BBB microvascular endothelial cells consist of three integral membrane proteins with many diverse cytoplasmic proteins help integral membrane protein connections to occur BBB properties. Claudin, occludin, and junction adhesion molecules (JAM) are integral membrane proteins. Claudin is the major TJ to determines the firm interconnection between BMECs. It also restricts small molecular transportation. There are 27 subtypes, with each ~26 kDa molecular mass. Claudin-5 is the most studied molecule that has barrier function. Lack of Claudin-5 in animal models makes BBB highly permeable to small molecules (< 800 Da). Reducing Claudin-5 expression level does not cause BBB disruption in their morphology. However, it causes harmful brain damage and can lead to death 10-hour after birth. Claudin-3 is also expressed in BMECs that have a function in the BBB. Claudin-11 and Claudin-12 have been discovered in BMECs. However, Claudin-12 does not have a significant role in the

BBB. Occludin is the first identified TJ protein in BMECs (Lochhead *et al.* 2020). It is a prominent component of TJs that forms dimerization and high-order oligomers. It is critical to BBB function. However, lack of occludin in mice causes growth disruption and histological abnormalities without TJs disruption in their structure and function. It is thought that tight junction-associated marvel proteins (TAMPs) could be replaced with occludin.

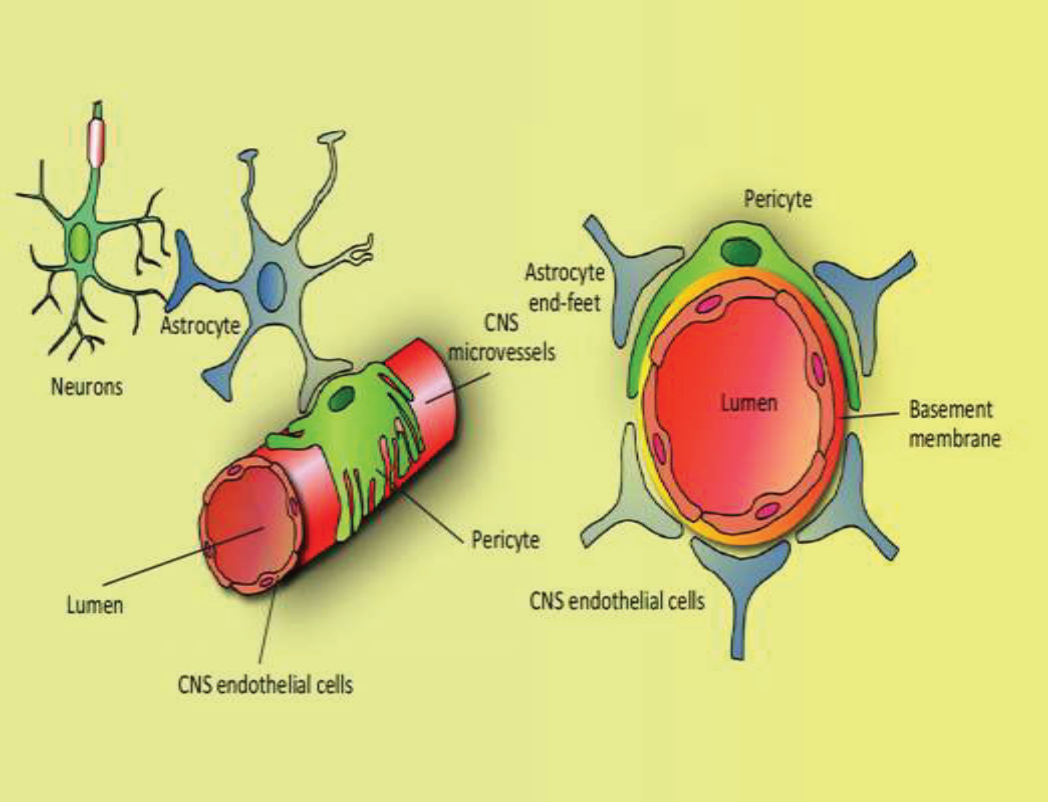

Figure 1.1. Blood-brain barrier cellular units with their localization around the endothelial cells. These cells are brain microvascular endothelial cells, pericytes, astrocytes and neurons. Basement membrane support those cells and regulate signaling cascade between endothelial cells and other cell types (Chow & Gu 2015).

Another study shows that the oligomerization disrupts increased permeability between BMECs. If the occludin transfected to cells that do not have TJs, cells demonstrate a similar structure to TJs. JAM is an immunoglobulin superfamily subtype of the integral membrane. They do not participate in TJs structure. However, it is critical to BBB function with the regulation of occludin binding to TJs. The barrier function occurred by tight junction and integral membrane proteins' organization and interactions

(Hamm *et al.* 2004). BBB integrity could only be supplied by suitable interactions of TJ integral membrane proteins that need several helper proteins to have proper function. An important one is zonula occludin (ZO), a membrane-associated granulated kinase family member protein. There are three different subtypes that bind and crosslink to several TJs and link between actin and TJs. These subtypes have sequentially difference in their C-terminals that makes them functionally different from each other (Lochhead *et al.* 2020). ZO-1 is the most studied molecule that connects tight junctions to the cytoskeleton. Thus, it has been directly implicated to TJ tightness. ZO-1 regulates the TJ stability and BBB integrity. ZO-2 is a transcription factor that binds TJ proteins to regulate their expression. Another subtype is ZO-3 found in ECs but, its function has not been well studied. The BBB property is highly connected to these TJs. Therefore, BBB dysregulation is also related to these proteins. Lack of barrier integrity has been reported in many different neurological diseases like traumatic brain injuries (Xu et al. 2017; Gerzanich *et al.* 2019), stroke (Metha, Tosun *et al.* 2015), Alzheimer's disease (AD) (Cai *et al*. 2018), Parkinson's disease (PD) (Desai *et al.* 2007), epilepsy (Marchi *et al.* 2012), and multiple sclerosis (MS) (Schattling *et al. 2012*). BBB integrity disruption causes impairment in ion dsyregulation and cellular signaling. It also increases the immune response in the CNS that exacerbates neuronal deficiency, degeneration, and progression of disease. For this reason, the maintenance of the BBB integrity could be considered as a therapeutic target for several neurological diseases.

1.2. Sulfonylurea Receptor

The sulfonylurea receptor (SUR) is a subtype of the ABC-binding cassette proteins. ABC proteins are highly conserved and are expressed in a wide range of organisms, from prokaryotes to eukaryotes. They use ATP as an energy source and supply the passage of nutrient import and/or remove toxins from cells. Even though they are highly conserved proteins, SUR is an atypical form of ABC protein because of its ion channel activity. There are 2 subtypes of SUR; SUR1 and SUR2, and SUR2 has subtypes SUR2A and SUR2B. SUR1 is expressed by the ABCC8 gene and is expressed in pancreatic ß cells and brain cells (neurons, astrocytes, microglia, oligodendrocytes, and microvascular endothelial cells). The ABCC9 gene codes for SUR2. SUR2A is expressed

is in the heart, whereas SUR2B is expressed in smooth vascular muscle cells. SUR1 consists of 3 transmembrane domains TMD and 2 ABC domains (Burke *et al.* 2008). TMD0 domain is specific to SUR that is located in the N terminal of SUR with 5 alpha-helicases and connected to TMD1 with a CL3 linker (Aittoniemi *et al.* 2009). Both TMD0 and CL3 linkers have a role in channel opening (Nichols 2006). SUR1 could be associated with other channel proteins to form a functional ion channel. Even though the two channels' structure and ATP dependence are similar, they have different properties in specific cells.

1.2.1. K_{ATP} channels

K_{ATP} channels regulate ion channels according to the metabolic condition of cells via sensing the ATP/ADP levels. They are heterooctomer composed of 4 subunits of SUR1 and 4 subunits of $K_{ir}6$. $K_{ir}6$ subunits are the pore-forming subunits that are arranged in a ring to form the core of the channel, while SUR1 subunits surrounds them to regulate the channel. The molecular mass of the total channel is about 950 kDa. K_{ATP} channels are found in many different organs and tissues like the pancreas, heart, vascular smooth muscle, and brain. According to their place, their subunits, and also their channel properties they differ from each other. SUR1-$K_{ir}6.2$ subunits are found in pancreatic beta cells to regulate insulin-release and in the brain for neuroprotective effect during ischemia or hypoxia (Li *et al.* 2017). SUR2A-$K_{ir}6.2$ subunits are expressed in the heart to protect cardiac myocytes (Grover, Garlid 2000). SUR2B-$K_{ir}6.1$ subunit are expressed in vascular smooth muscles for vasodilation (Hansen 2006).

ATP sensitive K channels with SUR1 and $K_{ir}6.2$ subunits are responsible for K^+ efflux causing hyperpolarization and insulin release in pancreatic B cells. A high level of intracellular Mg-ADP causes channel opening (Principalli *et al.*2015). On the other hand, a high level of ATP causes channel closing with depolarization of the cell and elevated K^+ level in cells. Depolarization results in Ca^{+2} channel opening to increase Ca^{+2} level inside the cells. The signal cascade ends up with the release of insulin from cells via the Ca^{+2}-dependent insulin release pathway. In diabetes mellitus type 2 (DM 2) disease, there is a reduced level of insulin uptake even though ATP levels are sufficiently high. For this

reason, Sur1 inhibitors have been successfully used to treat DM 2 for more than 40 years to depolarize cells (Szeto *et al.* 2018).

In neuronal cells, ATP depletion leads to opening of K_{ATP} channel and depletes membrane potential to decrease cell excitotoxicity that has a cytoprotective effect. During ischemia, hyperpolarized cells have a potential escaping cell death and excitotoxicity (Sun, Feng 2013). For this reason, K_{ATP} channel openers such as diazoxide have been investigated as a potential neuroprotective drug. Treated rodent models show a smaller infarct volume and damage after an ischemic stroke (Shimizu *et al.* 2002). Contrarily, K_{ATP} channel blockers like tolbutamide are expected to exacerbate infarct volume (Zhang *et al.* 2016). However, glibenclamide that is a blocker of SUR1 shows less infarct volume with an improvement in neurological conditions in the rodents after ischemic stroke (Wu *et al.* 2016). The reason is that another channel of SUR1 is associated with TRPM4.

1.2.2. SUR1-TRPM4 channels

Transient receptor potential (Trp) is a superfamily of non-selective cation positive monovalent, and divalent ion channels with 28 subtypes (Nilius *et al.* 2009). Two subtypes of Trp have an unordinary function that transportation of monovalent ions. However, divalent ions (Ca^{+2}, Mg^{+2}) do not pass the channel. These are transient receptor potential melastatin 4 (Trpm4) and Trpm5 (Mahtar *et al.* 2014). Under normal conditions, Trpm4 is not expressed in the CNS (Kunert-Keil *et al.* 2006). However, injury to the CNS cause an increase *de novo* expression of Trpm4 like SUR1 (Simard *et al.* 2009). In 2013, the Sur1 and Trpm4 channel's direct association has been reported with regulation of intracellular the Ca^{+2} and ATP levels (Woo *et al.* 2013). SUR1-TRPM4 channels form a heterooctomer and are composed of 4 subunits of SUR1 and 4 subunits of Trpm4. Trpm4 is at the core of the channel, forming the pore-forming subunit, similar to $K_{ir}6.2$ in K_{ATP} channels. SUR1 is the regulatory subunit of this channel (Martines-Valverde *et al.* 2015). Cytosolic Ca^{+2} rise and ATP depletion inside the cell trigger channel opening causes Na^{+} influx, and thus cell depolarization (Vennekens, & Nilius 2007). Trpm4 has a calmodulin-binding site at the end of the C side. The regulation of Trpm4 channel opening occurs via calmodulin (Gerzanich *et al.* 2018). The depolarization causes cytotoxic edema and oncotic cell death (Simard *et al.* 2012). The

cellular edema is regulated by the SUR1-Trpm4 channel's co-association with the aquaporin-4 water channel for water influx in astrocytes (Stokum *et al.* 2018).

In 2001, Chen and Simard's colleagues reported SUR1-Trpm4 channels expression in native type R1 astrocytes in adult rats are exposed to hypoxic/ischemic conditions. They also revealed the opening of this channel was not maintained by either ADP or AMP, but only with by ATP (Simard *et al.* 2010). ATP depletion and reactive oxygen species (ROS) accumulation also causes oncotic cell death that disrupts BBB integrity. Redistribution of ZO-1 and MMP-9 secretion by neighboring cells in the damaged area has been associated with BBB breakdown process via SUR1-Trpm4 channels. MMP-9 is an endopeptidase that triggers disruption of extracellular matrix and causes BBB breakdown in many CNS disorders. They are secreted by mostly neutrophils, but also neurons, glial, and ECs. In BMECs, MMP-9 secretion is regulated by tissue plasminogen activator (tPA) (Marshall *et al.* 1979) traumatic brain injury models in rats (Xu *et al.* 2017). The upregulation of the SUR1-Trpm4 channel has been associated with the BBB breakdown and also, ionic and vasogenic edema in multiple sclerosis (MS), SAH, and cerebral infarct patients with a case of hemorrhagic transformation (Tosun *et al.* 2013).

SUR1-Trpm4 channels are associated with many different CNS disorders. The upregulation of this channel in MS is shown especially in astrocytes. In MS, inflammation, myelination, oligodendrocyte maturation, and axons are affected by channel upregulation progress disease (Makar *et al.* 2015). Channel upregulation in SAH has been related to BBB breakdown, ZO-1 distribution, and neuroinflammation (Simard, Woo *et al.* 2009). Glibenclamide in the intracerebral hemorrhage (ICH) rat model has reduced edema and MMP-9 secretion that stabilized BBB integrity (Jiang *et al.* 2017). Similar results were also shown in traumatic brain injury (TBI) and spinal cord injuries (SCI) (Gerzanich *et al.* 2019, Simard *et al.* 2007). SUR1 expression has also been found in cerebral metastases to decrease blood tumor barrier permeability (Thompson *et al.* 2013). In brain cancers, SUR1 inhibition potentially treats neuroinflammation decrease cerebral edema and neuronal homeostasis (Thompson *et al.* 2018). Stroke is a fatal disease because of its secondary damage to the brain that is incurable. SUR1-Trpm4 channels have a role in the regulation of this secondary damage. For this reason, blockage of SUR1-Trmp4 channels has an effective role in the treatment of hemorrhagic stroke and cerebral edema (Khanna *et al.* 2014). In hemorrhagic stroke, toxic hemoglobin releases cause oxidative stress and worsens the brain damage after ischemic stroke (Karsy *et al.* 2017).

1.3. Hypoxia Inducible Factor1 (HIF1)

HIF1 is a heterodimeric transcription factor that regulates cell adaptations to a hypoxic environment (Zhang *et al.* 2018; Wang *et al.* 1995). Hif1-α and HIF1-ß are the two subunits of the HIF1 and their molecular chemistry are a basic helix-loop-helix (bHLH) and Per-Aryl Hydrocarbon Receptor Nuclear-Sim (PAS) structure. Both subunits contain bHLH, PAS, N-Transactivation domain (TAD), and C-TAD domains. In addition, Hif1-α has an oxygen-dependent degradation domain (ODDD) that carries out its degradation process. Heterodimeric formation occurs by the bHLH and PAS domain interaction. PAS domain is also essential to DNA binding. Coactivators like CREB binding protein (CBP) and p300 bind to TAD domain to increase the expression of target genes in Hif1-α. In HIF1-ß, TAD regulates the target gene selection (Bogdanovski *et al.* 2017). Hif1-α is typically found in the cytoplasm and is degraded in basal normoxic conditions. When Hif1-alpha is not degraded, it indicates that the cell in a hypoxic environment and will translocate the transcription factor to the nucleus and dimerize with HIF1-ß. Dimerization causes HIF1 transcription factor activity in the genes that have Hypoxia Response Elements (HRE). The sequence of HRE is highly distinctive; 5' RCGTG 3'. HRE has been reported to be in more than 100 genes that are essential for the adaptation to hypoxic conditions (Kunze *et al.* 2012). Hypoxic adaptation occurs both in cell and tissue-specific manner.

Hif1-α is tightly regulated with many post-translational modifications that regulate the transcription factor HIF1 in the nucleus. These post-translational modifications are hydroxylation, ubiquitination, acetylation, phosphorylation, and SUMOylation. In normoxic conditions, Hif1-α hydroxylated immediately in the cytoplasm. The hydroxylation process is done by Prolyl-hydroxylase domain 2 (PHD2) that is dioxygenase. PDH2 breaks down O_2 atom and one transfer to 2-oxoglutarate (2OG) to produce succinate and CO_2. The other oxygen atom passes to proline residue of Hif1-α on the ODDD at 402 or 564 sites. O2 and Fe^{+2} are the coactivators of PDH2 and, their absence causes the inactivation of hydroxylation reaction. Ascorbate is another helper to this reaction because of its ability to the preservative of Fe^{+2} status. PDH2 activity inhibited by O_2 deprivation, citric acid cycle intermediates, and Fe^{+2} chelators such as cobalt chloride. Acetylation is another modification that increase VHL binding to hydroxylated Hif1-α. Acetylation occurs in the ODDD at 532 lysine residue by acetyl-

transferase. Hydroxylated Hif1-α binds to von Hippel-Lindau (VHL) protein-specific alignment between a hydroxylated part of Hif1-α and VHL protein. VHL binds to the E3 ligase complex is made of elongin C, elongin B cullin-2, and Rbx1 proteins. This binding triggers ubiquitination to degrade Hif1-α by 26S proteasome degradation pathway. During normoxic conditions, the interaction between Hif1-α and its coactivator is blocked by Factor Inhibiting HIF1 (FHIF1). FHIF1 hydroxylate C-TAD at 803 asparagine residue (Ke & Costa 2006). FHIF1 is another dioxygenase that reacts with alpha-ketoglutarate and O_2 to produce succinate and CO_2 (Semenza 2007). The regulation of Hif1-α production alters the phosphorylation of Hif1-α by p42/44 or p38 kinases. This phosphorylation does not influence Hif1-α stabilization or transcription. These post-modifications regulate O_2 dependent degradation mechanisms of Hif1-α. On the other hand, degradation could also occur in an O_2 independent pathway. Receptor activated C kinase 1 (RACK1) and heat shock protein 90 (HSP 90) binding to Hif1-α trigger the ubiquitination and proteasomal degradation.

HIF1 is a critical transcription factor that regulates cellular metabolism during hypoxic and ischemic conditions in the CNS. HIF1 is expressed in a biphasic pattern; in the early phase and late phase. In the early part, HIF1 typically regulates maladaptive cellular responses that occur within 4 to 8 hours. However, adaptive responses are then regulated at the late part that can take place between days 2 to 6 (Yeh *et al.* 2011). Nevertheless, the biphasic pathways exact reason and mechanism is not known. The potential reasons could be the severity and the duration of the hypoxia. Another reason could be the specific cell type in the organism. 30-minute ischemia in mice is sufficient to activate cell survival pathways. In that scenario, HIF1 activation has been shown to be neuroprotective (Baranova *et al.* 2007). Other researchers have reported that 75-minute of ischemia elevate the damage to the brain and is associated with the accumulation of HIF1. For this reason, Hif1-α knockout mice have reduced infarcts in their brain after injury (Helton *et al.* 2005). HIF1 could show a neuroprotective effect when the hypoxic conditions are mild. If the hypoxia is severe, HIF1 could exacerbate brain damage with apoptotic cell death and pro-inflammatory responses. Another reason for the biphasic response is the cell type-specific HIF1 downstream genes (Yan *et al.* 2011). In neuronal cells, HIF1 transcribes protective genes but, in the ECs it transcribes maladaptive response genes that cause BBB dysfunction (Sarkar *et al.* 2019). According to cell type hypoxia could give adaptive or maladaptive responses that could regulated by HIF1.

1.3.1. HIF1 adaptive responses

HIF1 has the potential to be neuroprotective via differential gene expression that can help adapt to a hypoxic environment. The underlying mechanisms are vasodilation, angiogenesis, energy metabolism, cell death escape, and erythropoiesis (EPO). HIF1 inhibits cytochrome c release, caspase activity, and p53 to avoid apoptosis (Sasabe *et al.* 2005; Zhang *et al.* 2011). However, p53 could also be activated by HIF1 when the ischemia severe (Piret *et al.* 2002). EPO regulates vasodilation and angiogenesis to take more oxygen from the vasculature. EPO has a role in apoptotic cell death regulation. In this way, neuronal cells are protected from hypoxic injury (Zaman *et al.* 1999). HIF1 also regulates glycolysis with glucose transporter boosting and increased glycolytic enzyme activity (Lawrence *et al.* 1996). Vascular endothelial growth factor (VEGF) is a key regulator of cellular survival mechanism and is directly transcribed by HIF1 (Liu *et al.* 1995). VEGF potentially upregulates cellular growth and differentiation in microvascular endothelial cells to maintain angiogenesis. In neurons, VEGF is also upregulated in an early and a late phase by HIF1. Therefore, drugs that upregulate HIF1 and VEGF

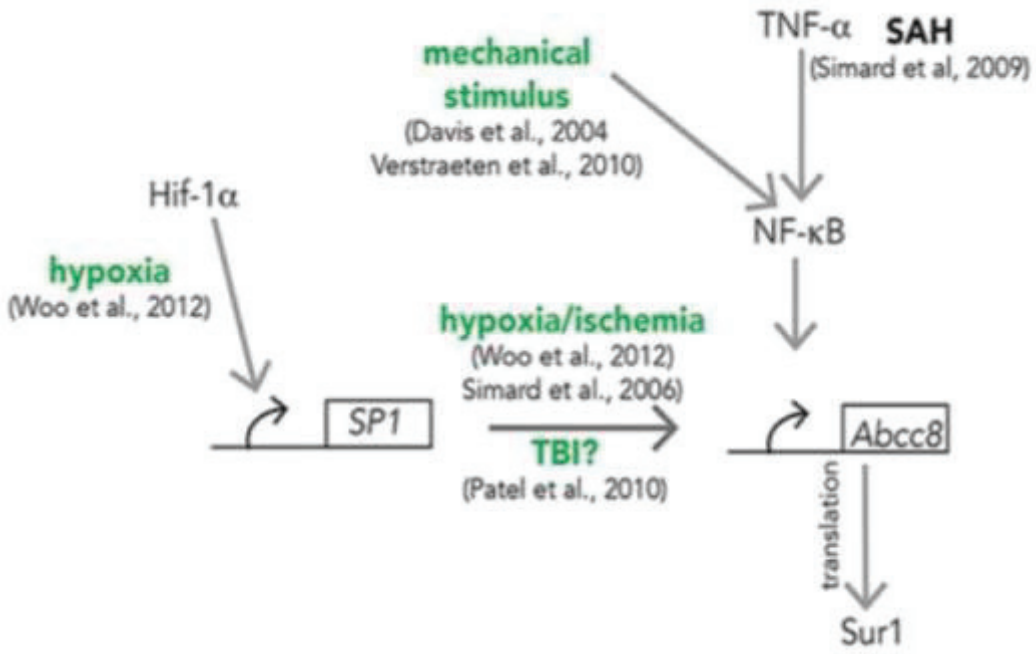

Figure 1.2. Schema show that Hif1-α and NF-kB activate Abcc8 gene to translate Sur1 during cerebral ischemia/hypoxia. Hif1-α indirectly upregulate Abcc8 gene via Sp1 transcription factor (Jha *et al*. 2020).

pathways have a therapeutic effect in neurons. 6 hours after TBI, deferoxiamine (DFX) has a neuroprotective effect by upregulating HIF1 and VEGF in rat model (Wang *et al.* 2020). In another study, HIF1 is upregulated three days after TBI with enhanced apoptosis. Sangi is Chinese medicine reduces apoptosis via the effect of the VEGF pathway (Yang *et al.* 2019). VEGF has also been associated with neurogenesis. It is regulated by Hif1-α accumulation and CREB phosphorylation. VEGF and NKCC1 mediate neurogenesis upregulated 8 hours after TBI and this increase is preserved for 7 days. In contrast to those researches, highly upregulated VEGF causes vessel leakage and vascular permeability (Zhang *et al.* 2018). For this reason, VEGF targeted therapies are also considered as novel neuroprotective strategies.

1.3.2. HIF1 maladaptive responses

In contrast to the adaptive response observed during hypoxia, an increased level of HIF1 can also cause detrimental effects that trigger apoptosis and inflammation. p53 and p21 stability is regulated by Hif1-α that regulates the cell cycle. The activation of p53 triggers apoptotic pathways in the cell via NOXA, PUMA, and Bax genes (Schuler & Green 2001). Kim *et al*. demonstrate that the inhibition of NOXA increases cell viability (Kim *et al.* 2004). Another apoptotic pathway is triggered by BNIP3 induced mitochondrial disruption via membrane depolarization and opened by MPTP (Chen & Chang 2009). BNIP and BNIP3 have HIF1 binding sites in their promoter region that demonstrates a direct regulation of mitochondrial dysfunction with HIF1 (Bruick 2003). HIF1 causes an increased amount of lactate dehydrogenase (LDH). LDH levels elevate the amount of lactate which is a cytotoxic molecule that triggers apoptosis (Semenza *et al.* 1996). Leucine-rich repeat kinase 2 (LRRK2) is another molecule that causes apoptosis in the cell, and it has an HRE region in its proximal promoter region. HIF1 induces LRRK2 and causes cellular death and inflammatory response in the brain (Bae 2018). Notch-1 causes cell death in neurons. The Notch gene has a direct binding capacity with HIF1. Thus, Notch-1 signaling is activated by HIF1(Cheng *et al.* 2014). Cytokines IL-20 and IL1beta are regulated by HIF1 cause inflammatory responses in the brain. HIF1 inhibition has a protective effect in ischemia because IL-20 secretion decreases. (Chen & Chang 2009). On the other hand, a bacterial infection could enhance Hif1-α. HIF1

upregulation activates the VEGF pathway, BBB integrity disruption, and bacterial migration from the vasculature to the brain parenchyma (Devraj *et al.* 2020). BBB dysfunction causes cerebral edema in TBI and ischemia. Cerebral edema has been associated with HIF1 activation induced by VEGF, MMP9, and AQP4, and AQP9 (Lee *et al.* 2013). HIF1 and AQP4/AQP9 is upregulated 48 hours after TBI (Ding *et al.* 2009). Upregulation of AQP4 and AQP9 has been demonstrated in another TBI research with functional outcomes. HIF1 induced AQPs result in cerebral edema, neuronal injury, and deficits in neurobehavior following injury (Shenaq *et al.* 2012)

Newly discovered SUR1/Trpm4 channel upregulation during cerebral injury (ischemic, hemorrhagic, or traumatic) has been indirectly associated with HIF1. The SUR1protein is transcribed from *Abcc8* does not contain the HRE region, but it has a specific protein 1 (Sp1) binding site. Sp1 is a transcription factor that regulates development, cell cycle, and differentiation during embryonic and postnatal development. However, it plays a critical role in many diseases (Safe *et al.* 2014). Some of the diseases are development of cancer, Huntington's Disease and Alzheimer Disease (O'Connor *et al.* 2016). Sp1 upregulation is associated with E3 ubiquitin ligase that decreases the p53 and apoptosis in a stroke rat models (Rodriguez *et al.* 2018). Sp1 upregulates neuroglobin to protect cells from neuronal injury (Van *et al.* 2019). Neuroglobin transcription is regulated by HIF1 indirectly, similar to SUR1. However, these two Sp1 transcription factors give adaptive responses following ischemia. On the other hand, HIF1 indirectly regulates the upregulation of SUR1/Trpm4 channel is a maladaptive response. Sp1 upregulation has been reported in stroke rat models as early as 3-hour post-injury (Simard & Chen *et al.* 2006; Yeh *et al.* 2011). The affinity of Sp1 to the *Abcc8* gene has been reported by Simard *et al.* Recently, Sp1 has been associated not only with SUR1, but also with aquaporin 4. In a recent study, Sp1 target antioxidant resveratrol (RSN) reduce cerebral edema while enhancing neurological behavior and survival rate in rat ischemia model (Alquisiras-Burgos *et al.* 2020).

1.4. Aim of the Study

The hypothesis of this study is that hypoxia induced Hif1-α translocation in brain endothelial cells could demonstrate morphological changes because of the membrane

depolarization via upregulation of SUR1-TRPM4 channels in an *in vitro* novel hypoxia chamber model. For this reason, our aim was to demonstrate morphological and biochemical changes with O2 dependent (Novel hypoxia chamber model) and independent ($CoCl_2$) hypoxia models. In the novel hypoxia chamber model the expression of Hif1-α, apoptosis marker (cleaved caspase 3) and NF-κB translocation to the nucleus in time dependent manner.

CHAPTER 2

METARIAL AND METHODS

2.1. Materials

All materials are listed below in the methods section according to their used methods.

2.2. Methods

2.2.1. Cell Culture

In this study, bend.3 cell line was used to investigate hypoxic conditions' effects on the endothelial cells. In addition to this, all the cell culture procedures were done under sterile conditions inside the hood.

2.2.1.1. Cell Culture Conditions

Bend.3 cells were grown in high glucose DMEM (Dulbecco's Modified Eagle Medium) (Biological Industries, 01-055-1A). Growth medium was also containing 10% fetal bovine serum (FBS) (Biological Industries, 04-127-1B), 1% L-glutamine (Biological Industries, 03-020-1B), and 100 U/ml Penicillin-Streptomycin (Biological Industries, 03-031-5B). The cells were seeded inside 100 mm X 15 mm petri dishes (Corning, 430167) until they were thawing. The cells were incubated at 37 °C containing 5% CO_2 incubator (Thermo Scientific, Steri-Cycle Incubator). The culture medium was

refreshed every 3 to 4 days.

2.2.1.2. Freezing Cells

Cells were counted with the hemocytometer to 7 X 10^5 cells inside the culture medium were transferred to cryovials with 0.1 ml dimethyl sulfoxide (DMSO) (AppliChem, A3672) and completed to 1 ml with FBS. The vials were stored at -20 °C for an hour before they were stocked in a -80 °C freezer (Nüve, DF490).

2.2.1.3. Thawing Cells

Stocked cells were removed from the -80 °C freezer, melted rapidly in a 37°C water bath (WiseBath, WB-22). Cells were plated into 100mm petri dishes and the culture medium was changed the following day and were kept until the confluency reached 80%.

2.2.1.4. Subculturing of the Cells

For the experimental procedures and continued growth of cell lines, cells were subcultured when they became 80% confluent. Before the subculturing procedure, the culture medium and 0.25% Trypsin – 0.02% ethylene diamine tetraacetic acid (EDTA) solution B (Biological Industries, 03-050-1B) was heated to 37 °C for proper enzyme function. Medium inside the cell culture was removed and cells were washed with culture medium. 2 ml of Trypsin-EDTA solution was added to a 100mm petri dish and was incubated for 5 minutes at a 37 °C incubator to allow cells to be detached. Cells were neutralized with equal volume (2 ml) of culture medium.

All cells and mediums were put inside 15 ml falcon tubes (Jet-Biofil, CFT-011-150) and centrifuged at 700 rpm for 10 minutes (Nüve, NF800R) at room temperature. The supernatant was removed and the pellet was dissolved in 1 ml of culture medium. 0.4% Trypan blue (Sigma, T6146) with PBS was prepared for cell counting with a

hemocytometer. Briefly, 16 µl cell suspension and 64 µl Trypan blue were mixed inside an Eppendorf tube and were immediately transferred to the hemocytometer and coverslipped. Cells were counted in the middle part of the squares with a compound inverted microscope (IX81, Olympus), and the average cell number in two squares were calculated. Calculated numbers were multiplied with the dilution factor (5) and the hemocytometer square volume (10^4). The result gave the total cell number inside 1 ml of medium. For the experiments and continued cell passages, cells were seeded into new culture plates with appropriate culture media and seeding numbers as shown in Table 2.1.

Table 2.1. The seeding numbers and culture medium amounts of different cell culture plates.

Cell Culture Plate	Seeding Numbers	Medium amount in plate
100 mm petri dish	400,000	10 ml
12 well plate	50,000	1 ml
24 well plate	25,000	0.5 ml

2.2.1.5. Trypan Blue Staining and Counting with Hemocytometer for Cell Viability

For the cell viability assay, cells were seeded to 12-well culture plates. After one day, the medium was changed with fresh complete culture medium, and cells were grown in hypoxic conditions (detailed below in sections 2.2.2.1 and 2.2.2.2) and normoxic conditions for 12 and 24 hours. Cells were then washed with medium and 100 µl Trypsin-EDTA solution was added to each well for trypsinization at 37 °C for 5 minutes. After that, cells were pipetted several times for detachment and neutralized with equal volume of culture medium. 40 µl of cells and 40 µl of trypan blue were mixed and counted using

the hemocytometer. Alive and dead cells were calculated for statistical analysis for cell viability. To calculate the percentage of cell death, dead cells were divided to the total cells number (dead and alive cell) and multiplied by 100.

2.2.2. Hypoxia Models

2.2.2.1. Inflatable Chamber Model

Hypoxic conditions can be created in a very practical and reproducible way that could be setup in every lab (Wang *et al.* 2014) For this purpose, we used a sterile resealable plastic zip-lock bag (IKEA) to create an inflatable chamber for hypoxia with a gas mixture composed of 1% O_2, 5% CO_2, and 94% N_2O_2 (Güneş Gas). 2 ports were

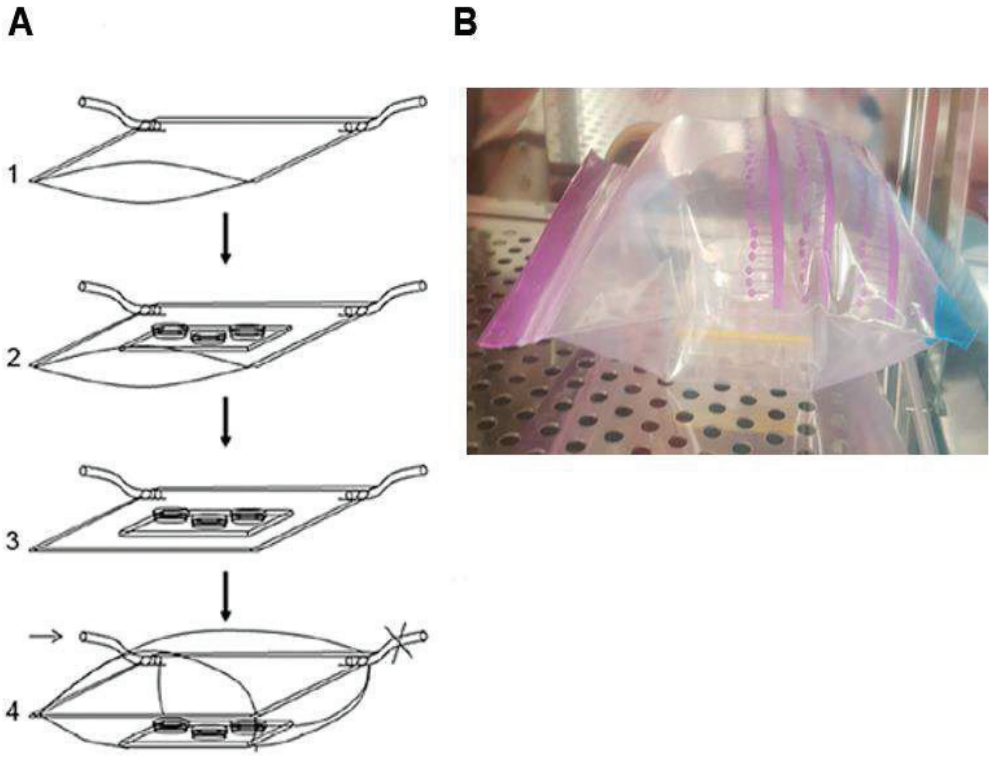

Figure 2.1. Novel hypoxia chamber model to mimic hypoxic environment.
A. Scheme of the inflatable hypoxia chamber model procedure step by step.
B. Example of the experiment, plastic bag contains cells that are exposure to hypoxia and water for humidity of environment (Wang *et al.* 2014).

opened in the bag and a glass Pasteur pipettes were inserted tightly to maintain airflow without any leakage. The cells were placed inside the bag with sterile water to provide a humid environment. A constant flow of the gas mixture was started to flow inside the bag. After making sure that the air inside the bag is replaced with the hypoxic gas mixture, one port was first closed, and the bag was filled until it reached 80% of its volume. Then, the other port is closed, heat-sealed and the hypoxic bag was placed inside the 5 % CO_2 incubator at 37 °C. At the same time, cells that were seeded at the same time and density were placed in the incubator to serve as normoxic controls. After putting the bags inside the incubator, the bags were controlled for several hours to make sure that they were not deflated, and no gas leak took place in/out of the inflatable chamber. Cells were exposed to hypoxic environments for different time points (4, 6, 12 and 24 hours) for further analysis.

2.2.2.2. $CoCl_2$ Treatment for Hypoxia Model

A chemically induced hypoxic environment could be induced independently of the O_2 concentration. $CoCl_2$ is a chemical inducer of HIF1 via blocking prolyl hydroxylases that degrade Hif1-α. Non-degraded Hif1-α translocate into the nucleus and HIF1 transcribes hypoxia response genes. In that way, the cellular metabolism is regulated as it was a hypoxic condition without reducing the O_2 amount in the environment. However, $CoCl_2$ is a cytotoxic molecule that harms cells without a hypoxic environment. Thus, it is critical to obtain a $CoCl_2$ concentration that is sufficient to cause a hypoxic condition without causing any cytotoxic effect. In the literature, suitable $CoCl_2$ concentration has been determined between 100-150 μM in bEnd.3 and other cell types (Chatard *et al.* 2017) For this purpose, in our experiments we used 50 μM, 100 μM, and 200 μM $CoCl_2$ concentrations.

To prepare the cobalt(II) chloride hexahydrate (Sigma-Aldrich), solution, appropriate amount of the chemical was dissolved in 1 ml of distilled water freshly before each experiment. It is critical to make sure that $CoCl_2$ is opened in a glowbox to prevent interaction with O_2 and maintain its chemical structure/integrity. Experimental cells were seeded in suitable plates and incubated for one day. After that, cells were washed with medium and fresh experimental medium was added into complete medium containing 50

μM, 100 μM, and 200 μM $CoCl_2$ in different wells. Cells were incubated at 37 °C 5 % CO_2 incubator for 4, 6 12, and 24 hours with their controls that did not contain $CoCl_2$ in their media.

2.2.3. Morphological Analysis

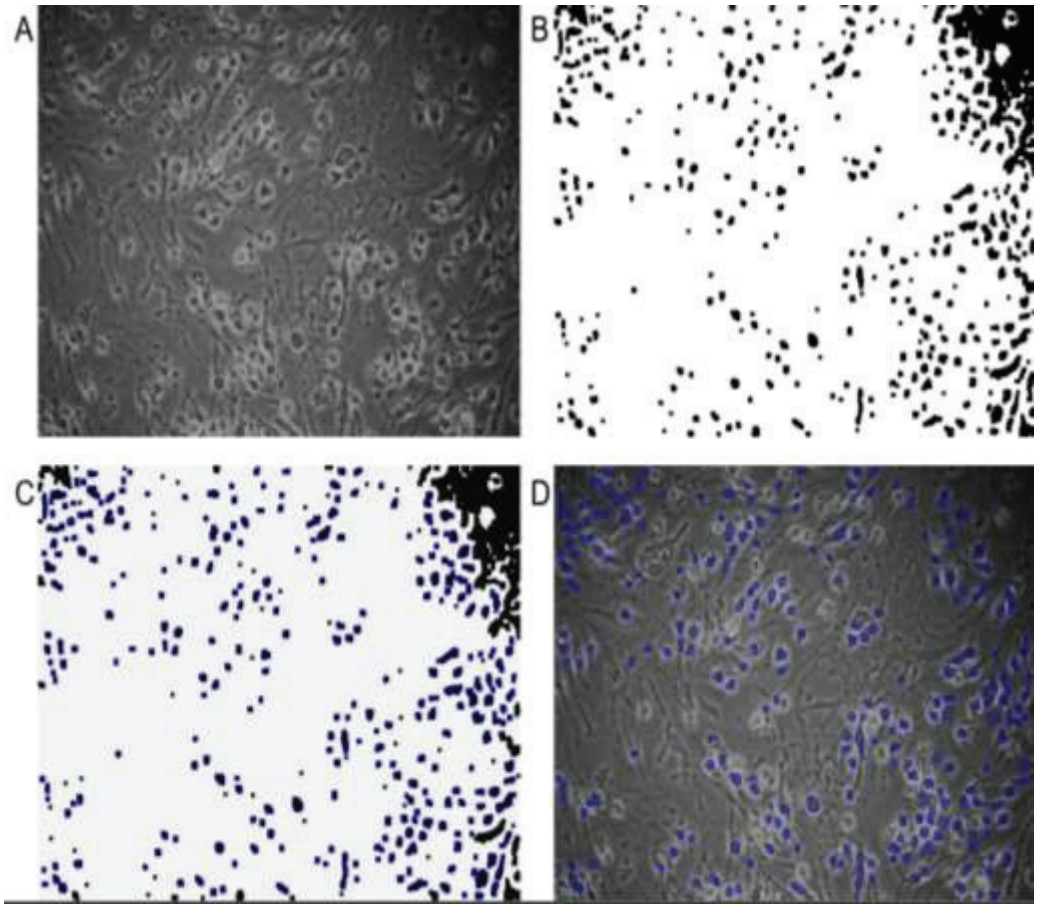

Figure 2.2. Morphological analysis with ImageJ program.

A. Bright-field image takes by an inverted microscope analyzed with ImageJ program.

B. Phalsankar auto local threshold of analyzed image with `Erode` and `Dilate` options.

C.Analyzed particles added to Region of interest (ROI manager).

D. Nonanalyzed images merged with ROI to control cells.

The circularity of the cell indicated by the yellow arrow is 0.274, by the white arrow is 0.971.

Cells were seeded at 2.5K inside 24-well plates for morphological analysis. Cells were incubated for one day in the 37 °C CO_2 incubator for attachment. Cells were then washed with medium and added suitable amount of fresh medium according to Table 1. Cells were exposed to hypoxic conditions and their normoxic controls for 4, 6, 12, and 24 hours. After that, cells were fixed with 4% PFA in PBS (Sigma, P6148) at room temperature for 20 minutes with gentle shaking. For morphological analysis, images were taken with an inverted microscope (IX81, Olympus) at 20X magnification with the bright-field mode after white balance. The pictures were analyzed by using the ImageJ program to determine their circularity for each cell (Figure 2.2). The images were adjusting for their brightness and contrast and was taken Phalsankar auto local threshold. The images were dilated and eroded, if necessary. Particles were analyzed with specific sizes between 30 and 400 $pixel^2$ and were added to the region of interest (ROI) manager. Each cells circularity was measured with the measure segment in the analyze particle section as shown below in Figure 2.2.

2.2.4. Immunostaining

2.2.4.1. Cell Staining with Antibodies

50,000 cells were seeded in 12-well culture plates. Cells were incubated at 37 °C, and one day later, cells were washed with medium and fresh culture medium was added to each well. Cells were exposed to the inflatable chamber model (hypoxic conditions and normoxic conditions) for 4, 6, 12 and 24 hours. After the completion of the experiments, cells were fixed with 4 % Paraformaldehyde (PFA) (Sigma, P6148) prepared in 1 X PBS at room temperature for 20 minutes on the shaker. All steps for immunostaining were incubated on the shaker (Thermo Scientific, 88881101) with 50 rpm shaking speed. Cells were washed with 1x PBS 3 times after fixation. Fixed cells were ready to be stained with antibodies: Hif1-α, Cleaved-Caspase 3, and NF-κB. Blocking solution was prepared with 2% BSA (1000mg/ml stock solution) with 0.2% TritonX-100 in PBS for an hour at room temperature for cell permeabilization. Primary antibodies were prepared inside blocking solution according to dilution ratio shown in Table 2. After the blocking was complete,

prepared primary antibodies were put on the cells and were incubated 1 hour at room temperature and then were placed on a shaker at 4 °C overnight. The next day, washing and secondary antibody staining were carried out at room temperature. The primary antibody was washed with 1X PBS for 3 times, 15 minutes each. Secondary antibodies were also prepared in blocking solution according to a dilution ratio shown in Table 2 according to appropriate species specific primary antibodies. For the negative control, a well was omitted the primary antibody and the secondary antibodies were added at the same dilution for the same incubation time. After that, all steps were carried out in the dark. Secondary antibodies were washed with 1X PBS 3 times, 15 minutes each. For nucleus staining, cells were stained with 0.05 % DAPI (0.01 stock solution) (Sigma,28718-90-3) in PBS for 15 minutes. DAPI was rinsed with 1X PBS and all images were captured with an inverted microscope (IX83, Olympus). 3 random images were captured from each well with the same magnification and exposure time, then analyzed with the ImageJ software program (NIH,).

Table 2.2. Primary and Secondary antibody list

Antibody	Ratio	Host	Brand	Catalog No
Cleaved Caspase-3	1: 200 for IF 1:1,000 for WB	Mouse	Cell Signaling	9661
GAPDH	1:10,000	Rabbit	Cell Signaling	5174
NF-κB	1:200	Rabbit	Santa Cruz	SC372
Hif1-α	1:200	Goat	Santa Cruz	SC13515
Goat anti-mouse	1:400	AlexaFluor 488	Invitrogen	A11029
Donkey anti-rabbit	1:400	AlexaFluor 555	Invitrogen	A31572
Donkey anti-goat	1:400	AlexaFluor 555	Invitrogen	A-21432

2.2.4.2. ImageJ Analysis of Immunostaining

Cleaved caspase-3, NF-κB, and Hif1-α staining was analyzed with overlapping DAPI staining to identify the specific signal within the nucleus. All the DAPI images were set to Threshold with the same values with the required Binary and were processed with Erode, Dilate, and Watershed under the tab of Process > Binary > Convert to Mask > Erode/Dilate/Watershed. DAPI images were analyzed under the Analyze > Analyze Particles tab. The selected options were summarized, added to the ROI manager, excluded on edges, and included holes. The DAPI stained nuclei were labeled and added to the region of interest (ROI manager). Analyzed images (NF-κB, Cas-3, Hif1-α) were arranged for their brightness and contrast under the tab of Image > Adjust > Brightness/Contrast. After that, show all options was clicked on the ROI manager. Finally, Measure was clicked on the ROI manager to identify the mean intensity (pixel) inside each nucleus. A threshold was set to for each labeling to create an unbiased way to analyze images and any value about the threshold was calculated as a positive cell. This number was then divided to the total number of cells in that image (with the DAPI staining) to determine the percentage of positive cells in that specific area. All images were captured at the same intensity and the parameters were set the same for each antibody staining when comparing experimental groups to their representative controls for image analysis.

2.2.5. Specific Protein Determination

2.2.5.1. Total Protein isolation

For the detection of protein levels with the Western Blot method, total proteins were firstly isolated from cells. Bend.3 cells were seeded to 100mm petri dishes and incubated for 4 days at 37 °C in 5% CO_2 incubator. After that, cells were exposed to hypoxic and normoxic conditions for 12 and 24 hours. Cells were then scraped with a cell scraper and collected inside a 15 ml falcon tube that was centrifuged at 4100 rpm for 5

minutes at 4 °C. After that, the supernatant was removed, and the pellet was dissolved in 200 µl complete medium. The sample was centrifuged at 5000 rpm for 5 minutes at 4 °C. The pellet was washed with cold 1X PBS and centrifuged again. The supernatant was removed and 50 µl of lysis buffer was added to each tube (Table 3) with 50X Protease Inhibitor Cocktail (PIC) (Roche; 04693159001). Lysis buffer was added to each sample and was incubated for 30 minutes on ice and was vortexed every 5 min. Then, these cells were centrifuged at 14.000 rpm for 15 minutes at 4 °C. Supernatants were then collected in another 1.5 mL Eppendorf tube to determine protein concertation using Bicinchoninic Acid (BCA) Protein Assay. Supernatants and pellets were stored in the -80 °C freezer.

Table 2.3. 2X Radio immunoprecipitation assay buffer (RIPA) Recipe

Component	Brand Name	Catalog Number
0.1 % Sodium dodecyl sulfate	Fisher Bio Reagents	BP166
% Triton X-100	AppliChem	9002-93-1
2 mM EDTA	Sigma	E5134
140 mM NaCl	Emsure	1.06404
10 mM Tris (pH:8)	AppliChem	77-86-1

2.2.5.2. Determination of Protein Concentration by Bicinchoninic Acid (BCA) Protein Assay

1, 0.5, 0.25, 0.125 and 0.0625 mg/ml Bovine Serum Albumin (BSA) (BioShop, ALB001.50) standards were prepared for strand curve. Sample proteins were diluted 1:10 ratio. 25 µl of BSA standards and diluted protein samples were loaded into a 96 well plates in triplicates with their blank. Water used as a blank. BCA (Pierce, 23227) solutions were prepared using reagents A and B according to manufacturer's instructions. 200 µl of the solution was added to each wells. The plate was gently shaken briefly inside the spectrophotometer. Solutions were then incubated at 37 °C for 30 minutes. The absorbance was read at 562 nm by a spectrophotometer (Thermo Scientific Multiskan Spectrum). Finally, to calculate the final protein concentration, after removing blank form

each absorbance value, we used the BSA standard curve and multiplied by the dilution factor.

2.2.5.3. Sodium Dodecyl Sulphate Polyacrylamide Gel Electrophoresis (SDS-PAGE) and Western Blot

12 % SDS-PAGE gels were prepared with resolving and stacking buffers. First, 10 ml of resolving gel was prepared with 4.7 ml water, 2.7 ml 30% acrylamide, 2.5 ml of 4X separating buffer (Table 4), 0.1 ml 10x APS (Sigma, 215589) and 6 µl TEMED (AppliChem, A1148). The prepared resolving gel was immediately poured between 1,5 cm glass plates and waited for complete polymerization. After that, 2.5 ml of stacking solution was prepared;1.425 ml water, 0.425 ml 30% acrylamide, 0.625 ml of 4X stacking buffer (Table 5), 25 µl 10x APS, and 5 µl TEMED. Prepared stacking gel was immediately poured onto the polymerized resolving gel and plastic combs were placed.

Protein concentration for all samples have been determined with BCA assay as detailed in section 2.2.5. 20 µg of total protein was loaded for each well. The protein sample was mixed with 5 µl of Loading dye (Thermo Scientific, R1151) and was adjusted to a final volume of 20 µl with water. Protein samples were then incubated in the water bath at 95 °C for 5 minutes for denaturation.

Gels were placed into western blot tank (BioRad Mini-PROTEAN Tetra Cell, 1658001) with 1X Running buffer (Table 6). All protein samples and 5 µl protein ladder (Thermo Scientific, 26619) were loaded into the gel and were separated first at 60 Volts for 30 minutes and then at 120 Volts for 60 minutes. The gel was gently removed between glass plates and was placed into the transfer sandwich. PVDF membranes were used for transfer. The transfer process took place in ice-cold 1X transfer buffer (Table 7) at constant ampere of 300 A for 90 minutes. When transfer was complete, the membrane was blocked with the blocking solution for an hour at room temperature. Blocking solution was freshly prepared with 5% non-fat milk powder (w/v) in phosphate-buffered saline 0.1% Tween-20 (PBS-T). The membranes were then washed with PBS 3 times and incubated with primary antibodies. Primary antibodies were prepared in blocking solution according to Table 8 based on Table 2 dilution ratios and stained overnight at 4°C gently rocking. The next day, membranes were rinsed 3 times in PBS-T, 15 minutes each.

Secondary antibodies were prepared in blocking solution with species specific horseradish peroxidase (HPR) (1:5,000) (Amersham, NA931). After one-hour secondary antibody staining at room temperature, the membrane was washed 3 times with PBS. Finally, target proteins were visualized and developed by ECL substrate working solution (Vilber, Lourmat Fusion fx7). Samples were normalized to GAPDH as a loading controls, and were quantified with ImageJ Software. The image was uploaded to the program, and all bands were selected to plot lines for quantification.

Table 2.4. 4X Separating Buffer Recipe for 200 ml (pH=8.8)

Component	Brand Name	Catalog Number
1.5M Tris base	AppliChem	77-86-1
0.4% SDS	Fisher Bio Reagents	BP166
dH2O		

Table 2.5. 4X Stacking Buffer Recipe for 200 ml (pH=6.8)

Component	Brand Name	Catalog Number
0.5M Tris base	AppliChem	77-86-1
0.4% SDS	Fisher Bio Reagents	BP166
dH2O		

Table 2.6. 10X Running Buffer Recipe for 500 ml

Component	Brand Name	Catalog Number
15 g Tris base	AppliChem	77-86-1
5 SDS	Fisher Bio Reagents	BP166
72 g Glycine	Fisher Bio Reagents	BP381
dH2O		

Table 2.7. 1X Transfer Buffer Recipe for 500 ml

Component	Brand Name	Catalog Number
1.5 g Tris base	AppliChem	77-86-1
7.2 g Glycine	Fisher Bio Reagents	BP381
20 % Methanol	Iron Kimya	
dH2O		

Table 2.8. Staining solution for 13 ml

Component	Amount
Wash Buffer (PBS-T)	12 ml
%5 Milk in PBS-T	1 ml
1000X Azide	13 ul

2.2.6. Statistical Analysis

All data is presented as mean ± standard error of mean (SEM). Student's t-test was used in Western blot analysis of cleaved caspase-3 in 12-hour experiment. Two-way Analysis of variance (ANOVA) with post-hoc Tukey analysis was used for all other statistical analysis. When the p value is less than 0.05 the difference was admitted as significant. All statistical analysis was performed using GraphPad Prism 5.0 (GraphPad Software, Inc., San Diego, CA).

CHAPTER 3

RESULTS

3.1. Determination of Cell Seeding Numbers for Further Experiments

To determine the proper cell death number in both models that we tested ($CoCl_2$ and inflatable hypoxia model) we wanted to first explore the growth rate of bEnd.3 cells. For this reason, we seeded 10,000, 50,000, and 100,000 cell per well in 12-well plates and incubated cells for 24 and 48 hours to observe the cell growth for this time-points. Experiments were conducted in four independent experiments (n=4) and statistical analysis was done using two-way ANOVA and Tukey posthoc analysis.

To identify the effect of serum in media, we also used the same time-points, but incubated cells with either complete media or serum-free media. Cells that was exposed to serum-free media had an overall reduction in the total cell number when compared to cells with complete media for the same time-points. In addition, serum-free cells had an overall increase in cell death percentages at every seeding number used in this study. For this reason, serum-free medium was not used in our experimental setup for further studies with $CoCl_2$ and inflatable hypoxia chamber models. At 10K cell seeding, the total cell numbers were not significantly different for both time points, 24 and 48-hours. On the other hand, cell death was significantly increased between 24 hours and 48 hrs. While the percentage of cell death at this seeding was 9.1% at 24 hours (Figure 3.1B), it was increased to 32.5% at 48 hours (Figure 3.2B). The reason for this difference could be because of the statistical error in the experiment because hemocytometer cell counting numbers were too low for the accuracy. At 100K cell seeding, the total cell number increased from 150K to 200K in 24-hour (Figure 3.1A). There was not a significant change in the percent cell death at 24 hours (9% to 12%). When cells were seeded at 50K, the total cell number increased 2 fold between 24 and 48 hrs. The percentage of cell death was less than 20% for both time-points observed. Cell death was 15.4 % for 24 hours and 18.3 % for 48 hours. Consequently, the cell seeding density was chosen as 50K for further analysis.

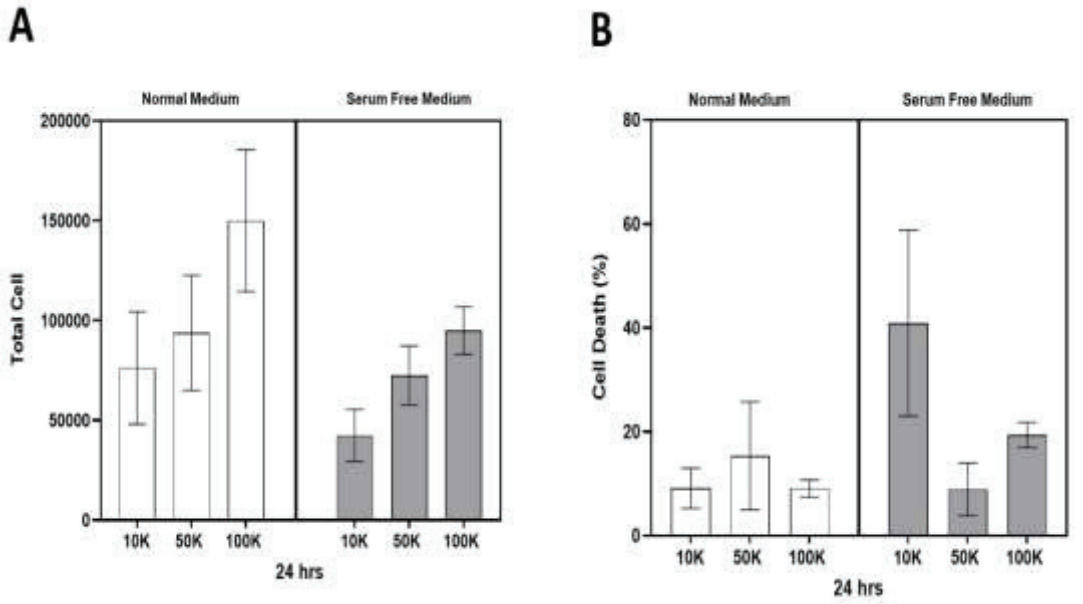

Figure 3.1. bEnd.3 cells seeded at 10K, 50K and 100K for 24-hour. Total cell numbers were calculated with Trypan blue staining (A). Cellular death percentage were calculated (B). Results are given as mean ± SEM; n=4. (*p<0.05; **p<0.01; ***p<0.001; ****p<0.0001).

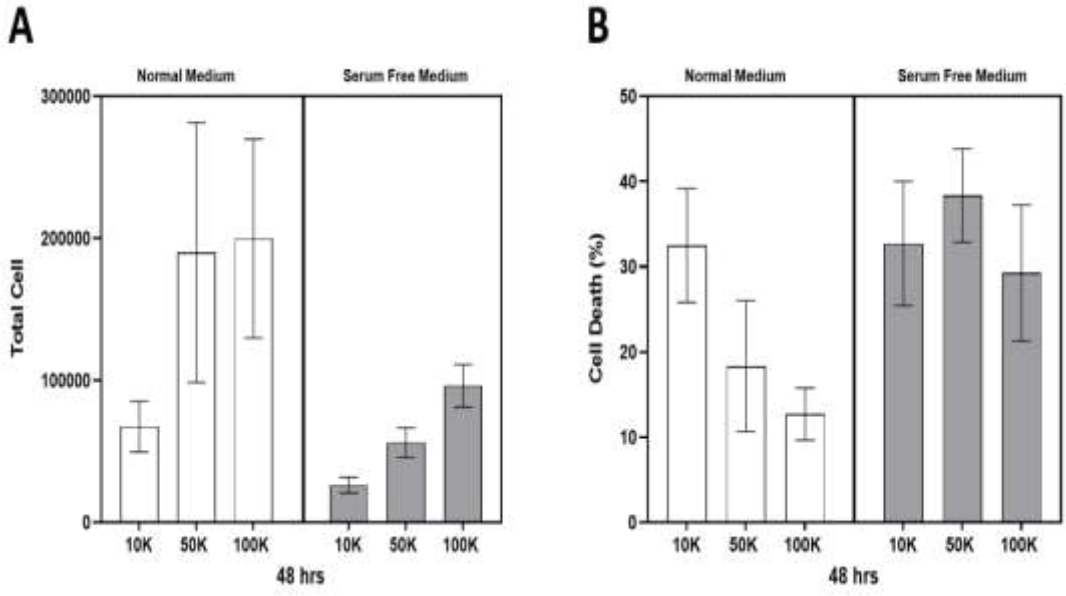

Figure 3.2. bEnd.3 cells seeded 10K, 50K and 100K for 48-hour. The calculated total cell numbers were quantified with Trypan blue staining (A). Cellular death percentage were calculated (B). Results are given as mean ± SEM; n=4. (*p<0.05; **p<0.01; ***p<0.001; ****p<0.0001).

3.2. Determination of the Cell Death in $CoCl_2$ Hypoxia Model via Trypan Blue staining

$CoCl_2$ is a chemical inducer of Hif1-α without the requirement of reduced O_2 concentration in the environment. $CoCl_2$ inhibits Prolyl hydroxylases that normally degrades Hif1-α. For this reason, we wanted to see the effect of cobalt-induced cell death via Trypan Blue staining. bEnd.3 cells were exposed to 50 μM, 100 μM, and 200 μM $CoCl_2$ for 12 and 24 hours. Before cells were counted on the hemocytometer, cells were trypsinized and stained with Trypan Blue to observe dead and alive cells. The percentage of dead cells and total cell numbers were calculated for control (no cobalt added to medium) and all $CoCl_2$ concentrations after 12 and 24-hour cobalt exposure. Experiments were conducted in three independent experiments (n=3) and statistical analysis were done using two-way ANOVA and Tukey posthoc analysis.

For both time points observed, we observed an increase in cellular death percentage with increased cobalt concentration. However, this trend did not reach significant. While there was no difference between the control group and 50 μM concentration for 12 hours, there was an increase from 7.2 % to 11.8 % with 100 μM $CoCl_2$ stimulation. However, it was not significant. Likewise, 200 μM $CoCl_2$ concentration significantly elevated cell death to 14.6 % when the compared to the control group. At 24-hours 100 μM $CoCl_2$ stimulation resulted in a slight increase of cell death from 2.8 % to 8.3 %. At the same time-point, 200 μM $CoCl_2$ concentration significantly increased cell death from 2.8 % to 13.3 % (Figure 3.3A). The total cell numbers significantly reduced for both 50 μM and 200 μM $CoCl_2$ exposure at 12-hours. At this time-point, the total cell number for control cells were 167 K, while it was reported to be 113 K for 50 μM and 125 K for 100 μM, and 108 K for 200 μM $CoCl_2$. 24-hour of $CoCl_2$ stimulation also caused reduced total cell number for all concentrations that were tested in this study. There was a significant decrease at 24 hours between control cells (155 K) to 100 μM and 200 μM $CoCl_2$ to 87 K and 95 K, respectively. (Figure 3.3B).

Overall, $CoCl_2$ was able to cause cellular death with increased concentration for 12-hour and 24-hour in bEnd.3 cells. During $CoCl_2$ exposure, cell death was not only increased, but also the total cell number was reduced. Additionally, 100 μM $CoCl_2$ concentration seemed to be suitable for further analysis because of its less cytotoxic effect compared to 200 μM.

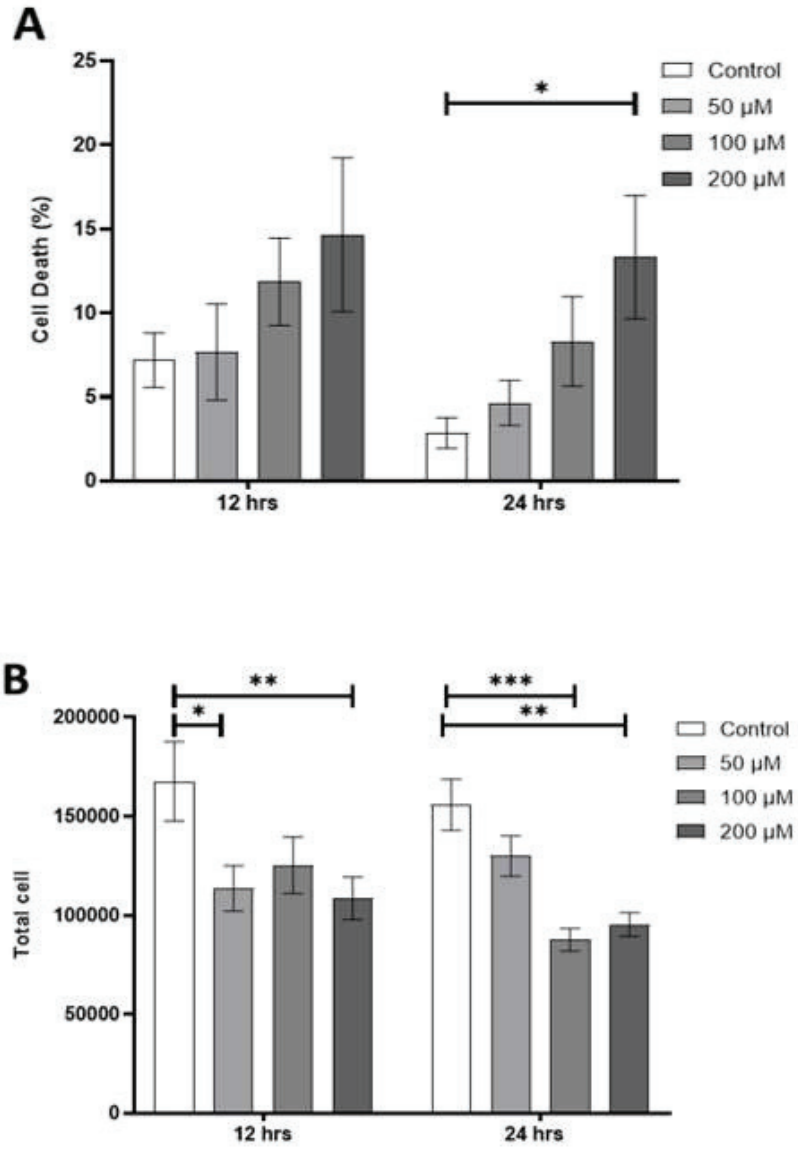

Figure 3.5. The effects of 12-hour and 24- hours of CoCl2 exposure in bEnd.3 cells in cellular death (A) and the total cell number (B). Control groups were not exposed to CoCl2. Results are given as mean ± SEM; n=3. (*p<0.05; **p<0.01; ***p<0.001; ****p<0.0001).

The morphological changes could be observed clearly after 6-hour exposure of 200 µM $CoCl_2$. However, all concentrations of $CoCl_2$ was sufficient to have a dramatic effect in cellular morphology after both 12 and 24-hours. Besides having an overall reduced cell number, the cellular shape observed more circular. However, these changes could not have quantified. On the other hand, these changes were not observed at earlier time-points at 4-hours in which cells were exposed to varying $CoCl_2$ concentrations (Figure 3.4).

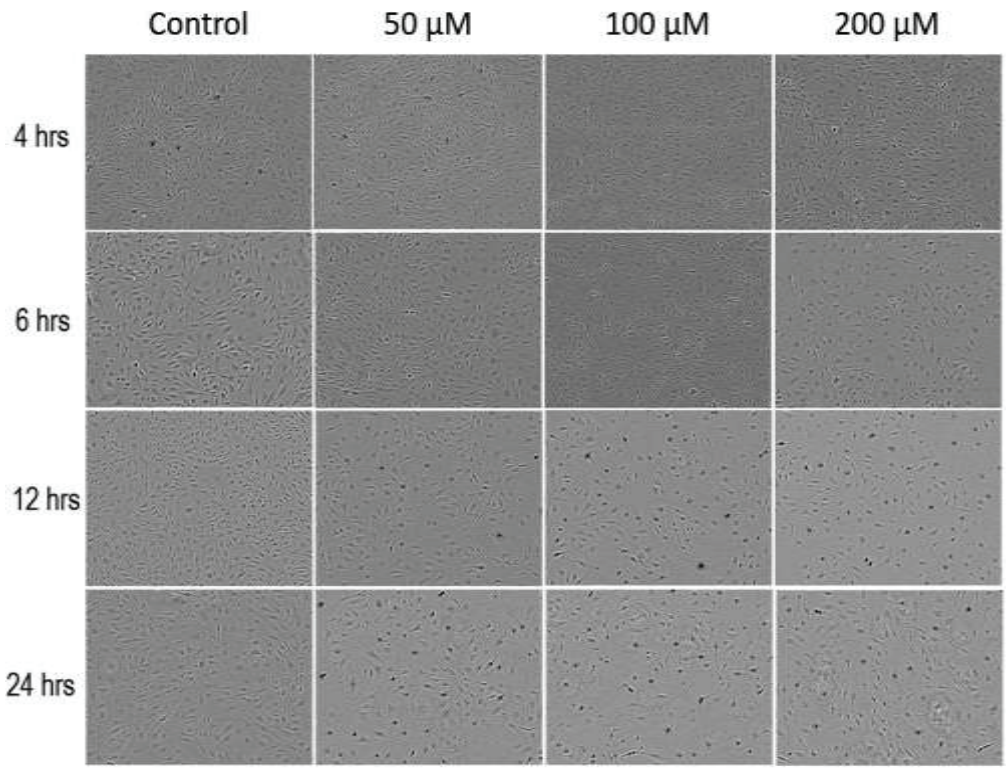

Figure 3.6. The cellular morphological changes after cells being exposure to 50 µM, 100 µM and 200 µM CoCl2 for 4, 6, 12 and 24-hour with their normoxic controls.

3.3. Determination of the Cell Death in Inflatable Hypoxia Chamber Model via Trypan Blue staining

bEnd.3 cells were exposed to hypoxic environment (1% oxygen) using an inflatable hypoxia chamber for 12-hour and 24-hours. After the hypoxic model was completed as described in Methods section 2.2.2.1, cells were counted on hemocytometer via Trypan Blue staining. Cell death percentage and total cell numbers were calculated. Experiments were conducted in five independent experiments (n=5) and statistical analysis was done using two-way ANOVA and Tukey posthoc analysis.

At 12 hours, hypoxic cells had a cell death percentage of 25.5%, while normoxic cells had a significantly reduced number at 8.4 % (Figure 3.5A). However, cells that were expose to 24-hours of hypoxia did not show a significant difference between the 2 groups; normoxia and hypoxia. At this time-point, cell death percentage was 9.5% for normoxia

and 11.5% for hypoxia. On the other hand, cell death was significantly reduced 0.45-fold in hypoxic cells between 12-hour and 24-hours. There was no noted change in the total cell numbers. The normoxic group had 105 K that was reduced to 86 K in the hypoxic group at 12-hours. On the other hand, normoxia had 116 K that was increased to 126 K in hypoxia at 24-hours (Figure 3.5B).

In short, the inflatable chamber model revealed a reproducible increase in cellular death at 12-hours. However, 24-hour of hypoxia did not show a significant change between normoxic and hypoxic conditions. Statistical analysis showed that the 12-hour of hypoxia significantly decreased cell viability when compared to 24-hours.

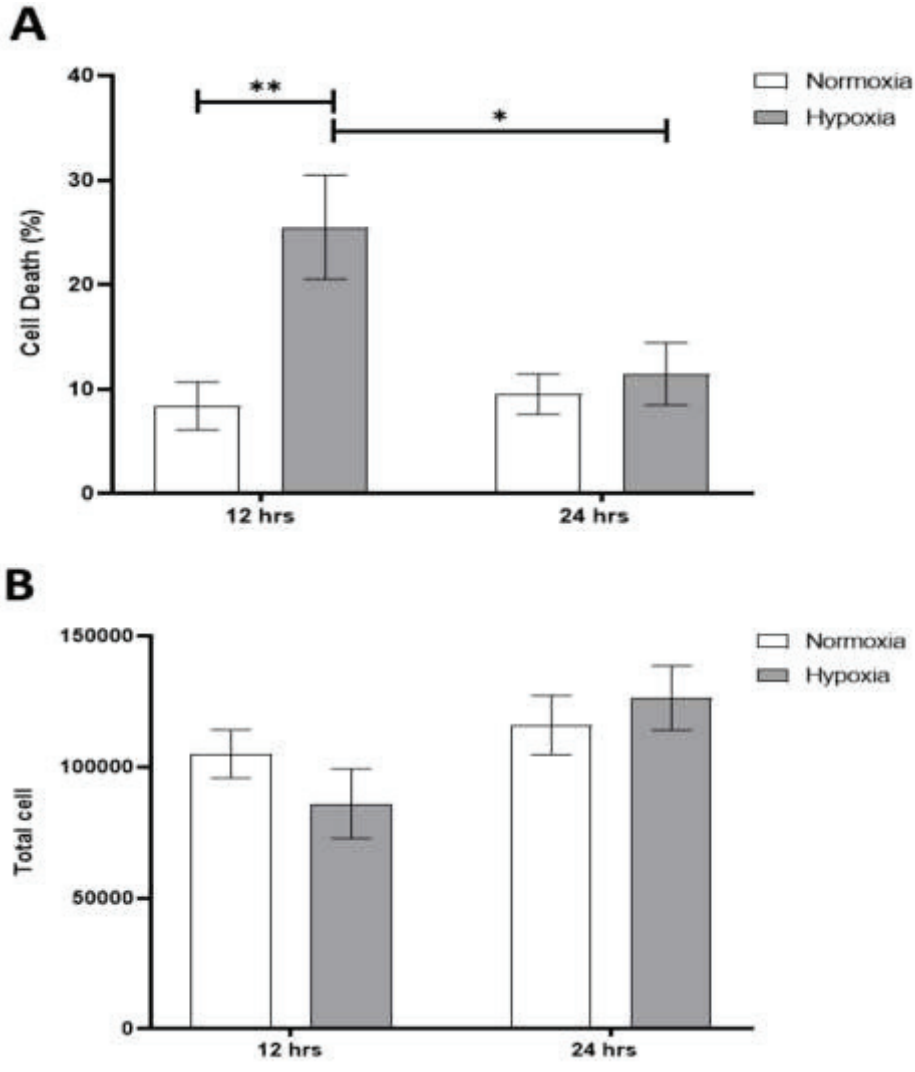

Figure 3.7. The effects of 12-hour and 24-hour of hypoxia in bEnd.3 cells in cellular death (A) and total cell number (B) with the inflatable hypoxia chamber model and compared to their normoxic controls. Results are given as mean ± SEM; n=5. (*p<0.05; **p<0.01; ***p<0.001; ****p<0.0001).

3.4. Characterization and Quantification of Cellular Morphology

Hypoxic environment was sufficient to cause a morphological change in bEnd.3 cells. The microscopic observation and the cellular circularity quantification can give us an idea about cellular stress conditions. For this reason, cells exposure the 4, 6, 12, and 24 hours of hypoxia and their microscopic images were taken for comparison. We observed dramatic changes between 12 and 24 hours so, we quantify the circularity of cells in each image with ImageJ analysis program mentioned Method 2. Analysis was executed in 3 independent images and repeated 3 times (n=3). Statistical analysis was done using two-way ANOVA and Tukey posthoc analysis.

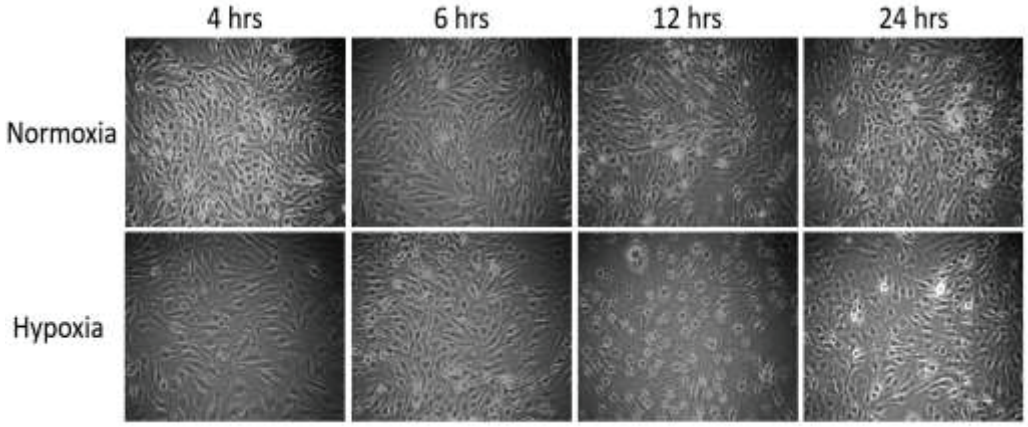

Figure 3.10. The cellular morphological changes after cells exposure 4, 6, 12 and 24-hour hypoxic environment with their representative normoxic controls.

The hypoxic environment caused the cells to shrink and to lose their characteristic spindle shape by deterioration. 4 hours of hypoxia did not have an effect in the cells morphology that could be observed or quantified. However, at 6-hour hypoxic cells began to shrink in size. Cells exposed to hypoxic environment for 12 hour showed that they were much smaller in size, circular in shape and mostly looked damaged. However, 24 hours of hypoxic cells looked similar to the morphology of 6 hours of hypoxia. On the other hand, normoxic cells had preserved their shape and structure at all time-points observed (Figure 3.6).

The cellular morphology was quantified with an analysis based on cell circularity. We created a histogram that quantifies the percentage of cells for each circularity in Image J as described, where 1 signifies a perfect circle. Cells that were exposed to 12-hours of

hypoxia showed a significant 1.2-fold increase between 0.9 and 1 circularities when compared to normoxic groups at the same time-point (Figure 3.7A). There were no significant changes between groups in their circularity index at 24-hours (Figure 3.7B). When hypoxic cells from 12 hours and 24 hours were compared with each other, the 24-hour had a significantly increase in the total number of cells that fell under the category 0.8-0.9 circularity (Figure 3.7C). In between that circularity, 22.3 % and 29.8 %. of cells fell in between that circularity at 12 and 24 hours, respectively. In addition, 24-hour hypoxia significantly reduced the number of cells in 0.9-1 circularity range. Cell circularity percentage was 40.7 % for 12-hour and 32.6 % for 24-hour in the hypoxic experiment. No significant differences in circularity was noted in normoxic groups at both time-points, indicating no observable stress in those groups.

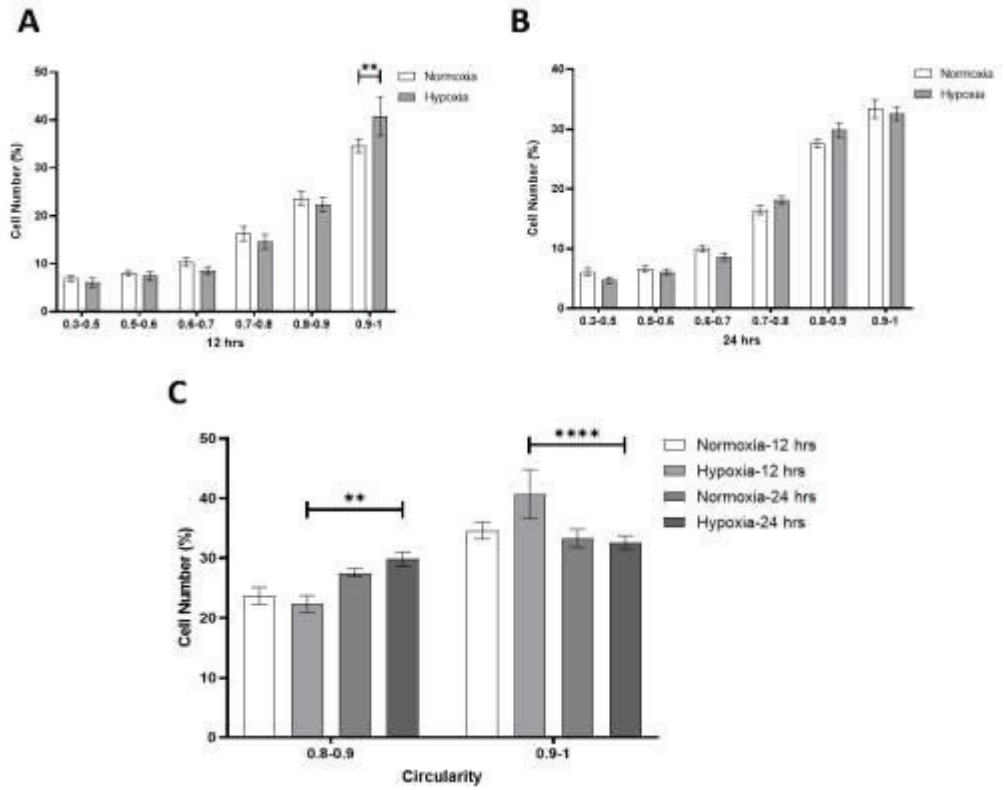

Figure 3.11. Quantification cellular circularity at 12 and 24 hours of exposure to hypoxia, compared to their controls. Cell circularity analysis at 12 hypoxic cells (B) for 24 hour hypoxic cells (C) with their controls. The comparison between 12 and 24-hour hypoxia circularity in two circular points which were between 0.8 and 0.9 and, 0.9 and 1 (D). Results are given as mean ± SEM; n=3.
(*p<0.05; **p<0.01; ***p<0.001; ****p<0.0001).

3.5. Time dependent changes of Hif1-α translocation after cells exposure to hypoxia

Hif1-α translocation was investigated by immunostaining after cells were exposure to hypoxia at 4, 6, 12 and 24 hours. All the time points were stained and their images were captured at the same time. Experiments were conducted in three independent experiments (n=3) and statistical analysis was done using two-way ANOVA and Tukey posthoc analysis.

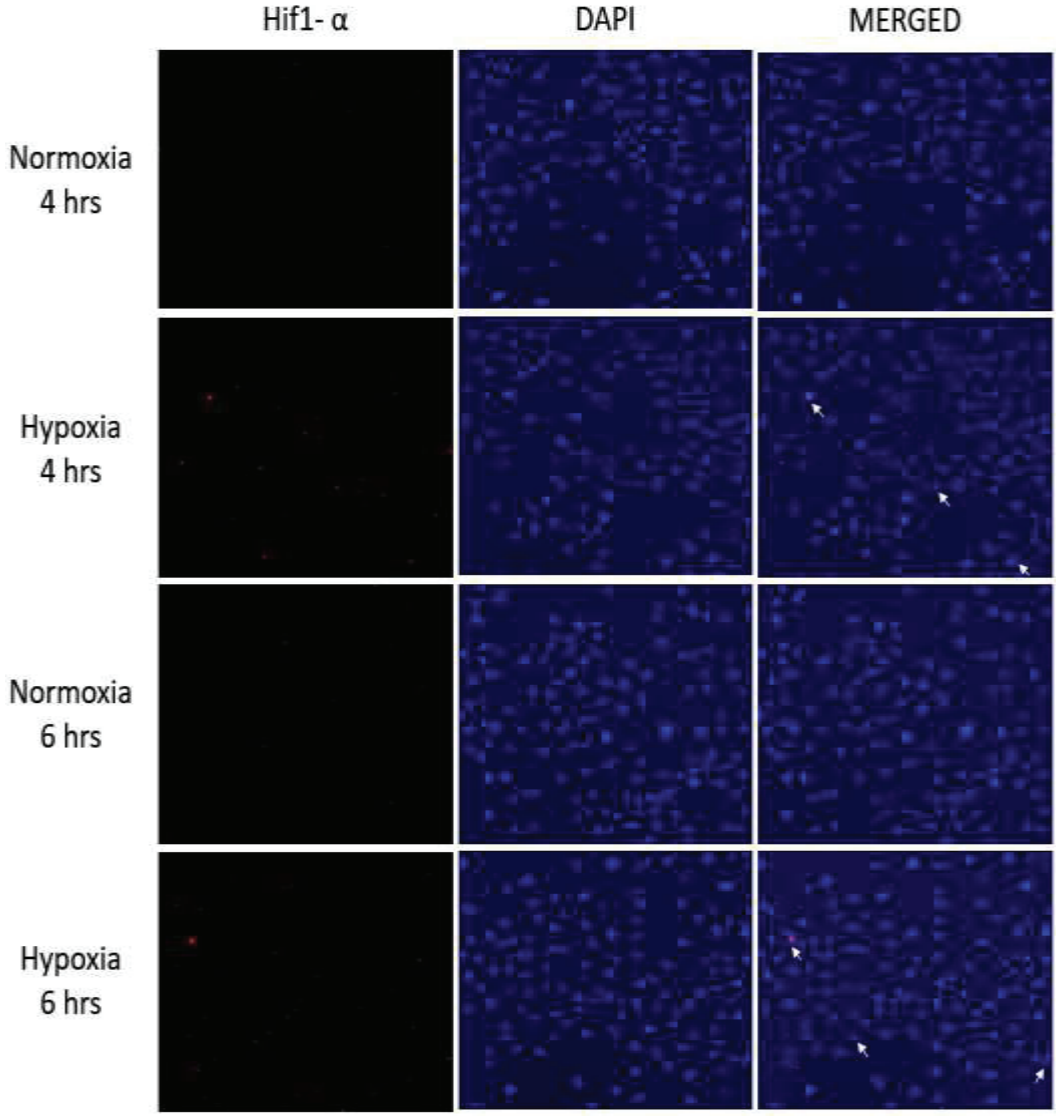

Figure 3.12. Hif1-α translocation observed by immunostaining in a time-dependent manner. Representative Hif1-α, DAPI and merged images are from normoxia and hypoxia for 4 and 6 hours. Arrowheads show Hif1-α translocation.

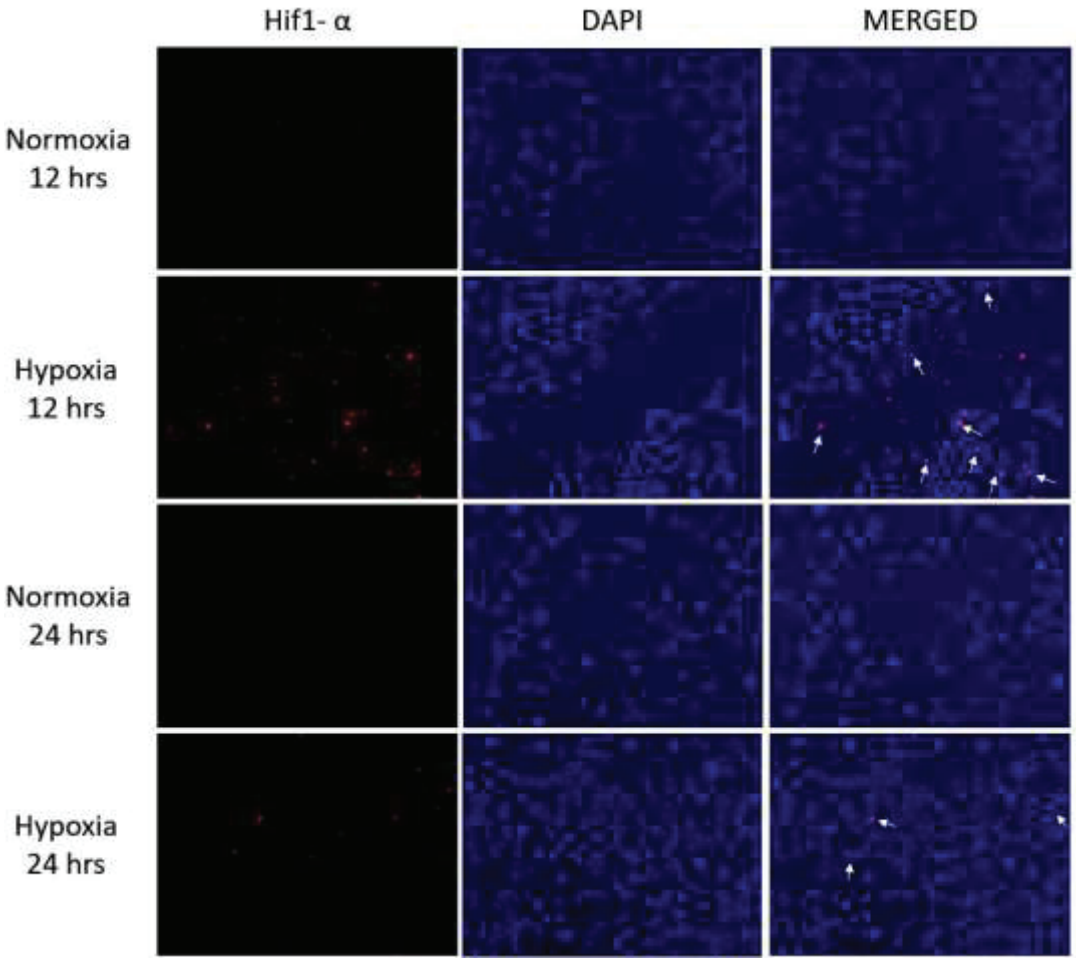

Figure 3.15. Hif1-α translocation observed by immunostaining in a time-dependent manner. Representative Hif1-α, DAPI and merged images are from normoxia and hypoxia for 12 and 24-hour. Arrowheads show Hif1-α translocation.

There was an increasing trend of Hif1-α nuclear translocation with increased duration of cells in hypoxic environment until 12 hours. (Figure 3.10). As Hif1-α is a common transcription factor that is upregulated rapidly after the induction of hypoxia, we wanted to verify that our inflatable chamber was able to effectively cause this translocation in bEnd.3 cells. 4-hour of hypoxia exposure was sufficient to cause 2.4 times more translocation of Hif1-α to the nucleus when the compared to normoxic controls. Similarly, 6-hour of hypoxia exposure resulted in a 2.2-fold increase in the translocation of Hif1-α. The significant increase was observed most prominently at12-hours of hypoxia where there was an increase of 27-fold in hypoxic cells when compared with their controls. There was also a noted significant increase between hypoxic groups between 4-hour and 12-hours, where there were more than 3 times the cells that had Hif1-α in their

nuclei at 12 hours. Interestingly, there was no significant change observed in cells exposed to hypoxic environment for 24 hours (p >0,9999).

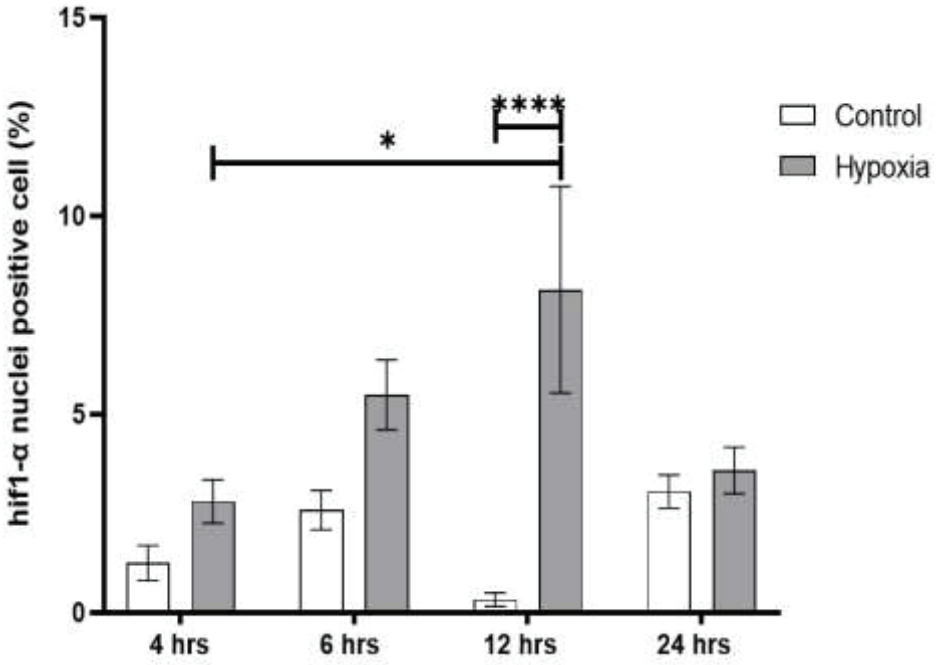

Figure 3.16. Quantitative of Hif1-α analysis of images demonstrated for 4, 6, 12 and 24-hour hypoxia. Results are given as mean ± SEM, n=3. (*p<0.05; ****p<0.0001)

3.6. Time dependent changes of NF-κB translocation after cells exposure to hypoxia

The nuclear NF-κB translocation was showed with immunostaining after the cells were exposure to hypoxic environments for 6, 12 and 24-hours. All time-points were stains and their images were captured at the same time. Experiments were conducted in three independent experiments (n=3) and statistical analysis was done using two-way ANOVA and Tukey posthoc analysis.

The bEnd.3 cells were expose to hypoxia for 6 hours show that not change NF-κB translocation when the compared with normoxic group (Figure 3.11). Likewise, 12-hour hypoxic cells also not noticeable change in the NF-κB translocation (Figure 3.12). In spite of that 24-hour hypoxic cells show significant rise in their translocation. 24-hour hypoxia

group was 12-times higher mean intensity than the normoxia group in the nucleus (Figure 3.13).

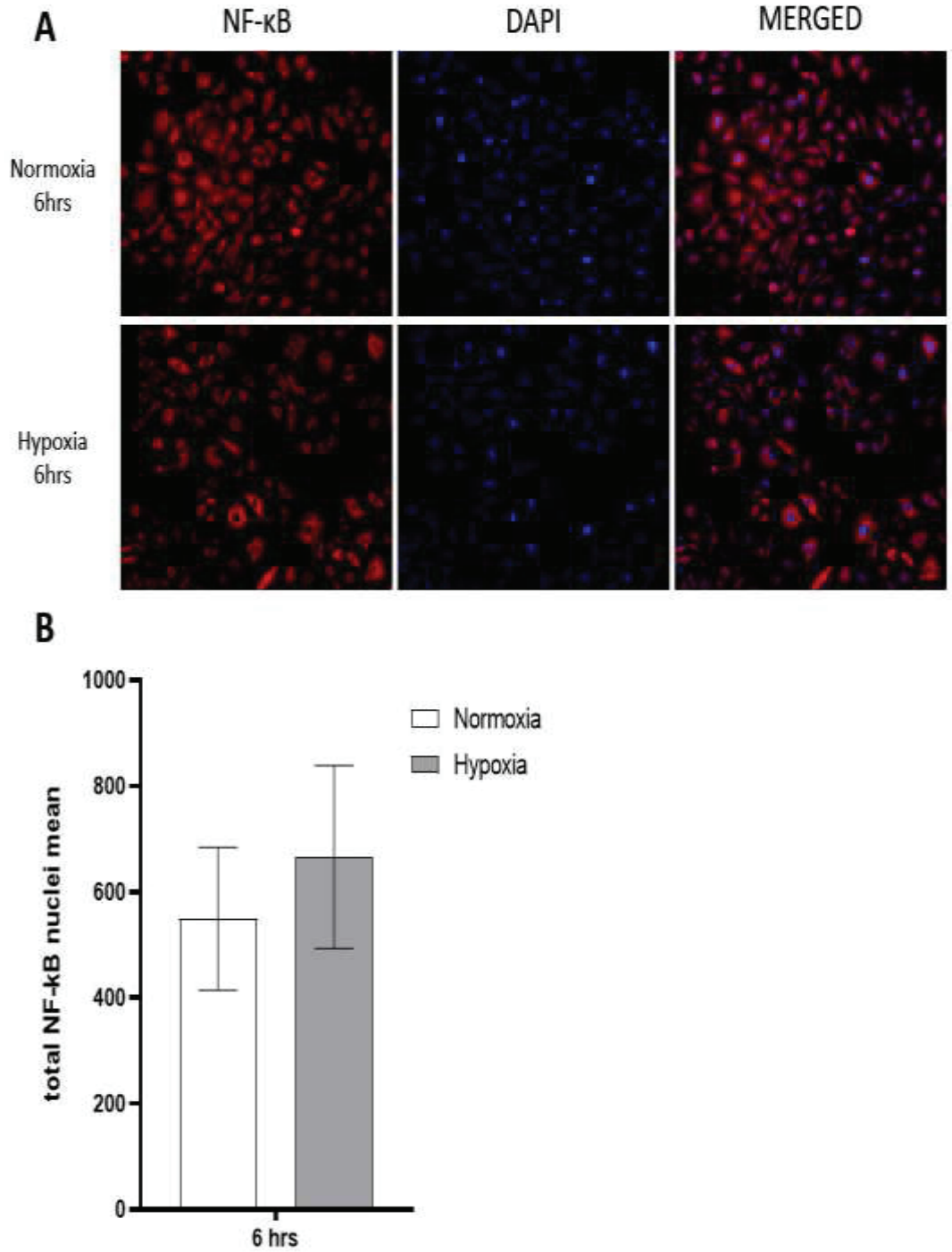

Figure 3.17. NF-kB translocation observed by immunostaining for 6, 12 and 24-hour hypoxia exposure.

A. Representative NF-kB, DAPI and merged images are from normoxia and hypoxia for 6-hour.

B. Quantitative data of the immunostaining of NF-kB for 6-hour. Results are given as mean ± SEM, n=3.

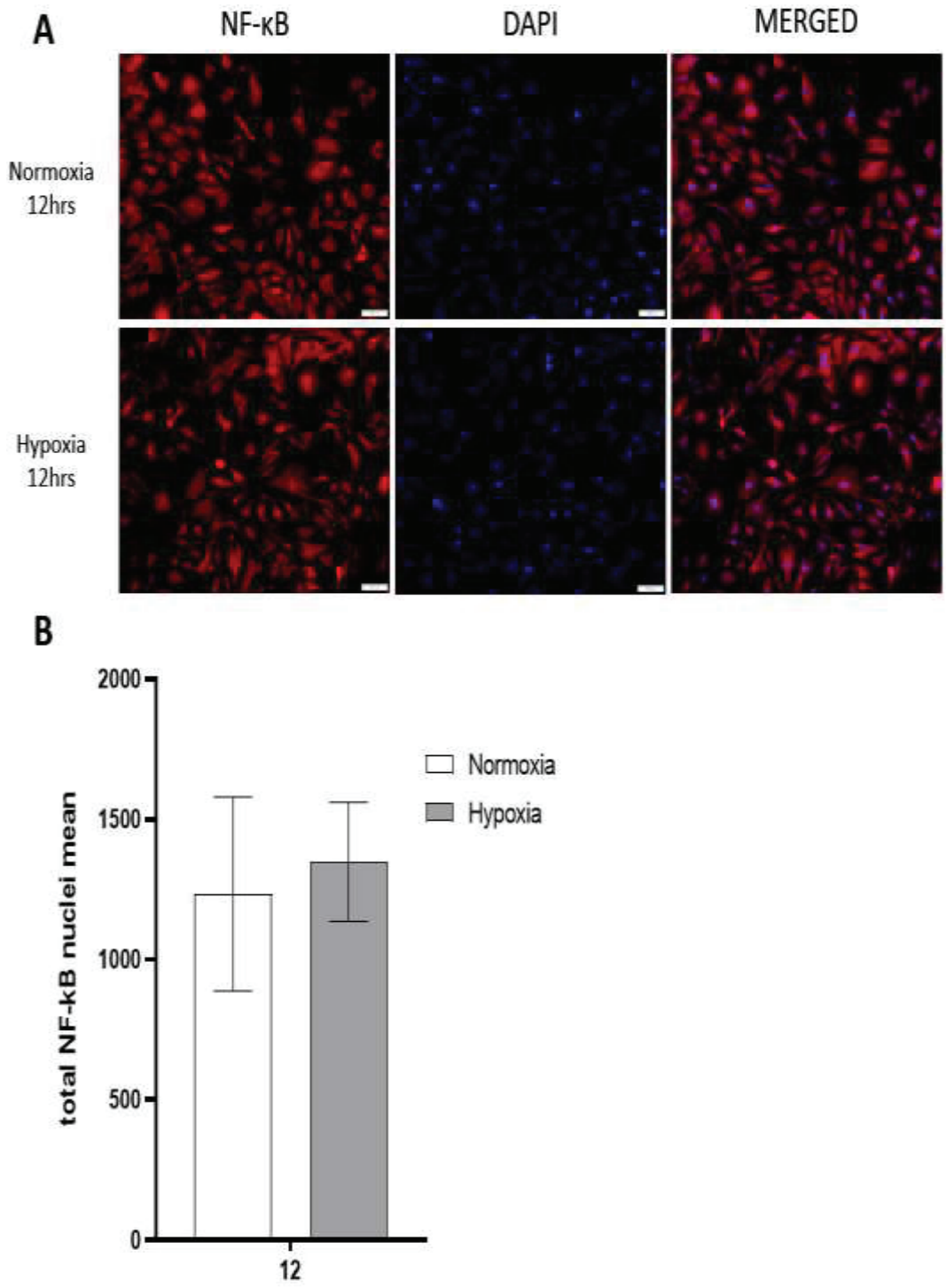

Figure 3.20. NF-kB translocation observed by immunostaining for 6, 12 and 24-hour hypoxia exposure.

A. Representative NF-kB, DAPI and merged images are from normoxia and hypoxia for 12-hour.

B. Quantitative data of the immunostaining of NF-kB for 12-hour. Results are given as mean ± SEM, n=3

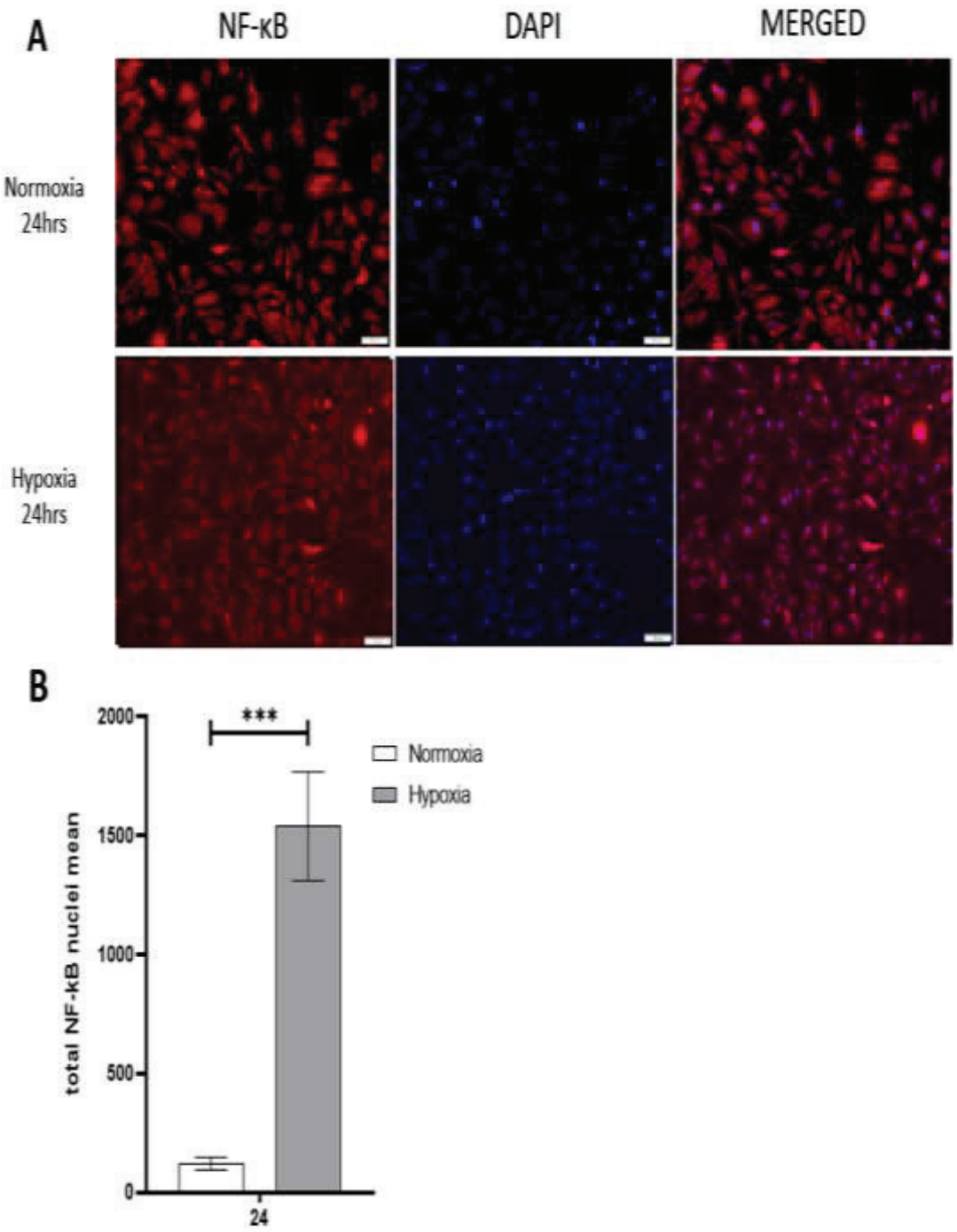

Figure 3.23. NF-kB translocation observed by immunostaining for 6, 12 and 24-hour hypoxia exposure.

A. Representative NF-kB, DAPI and merged images are from normoxia and hypoxia for 24-hour.

B. Quantitative data of the immunostaining of NF-kB for 24-hour.

Results are given as mean ± SEM, n=3 (***$p<0.001$)

3.7 Time dependent changes of cleaved caspase-3 translocation after cells exposure to hypoxia

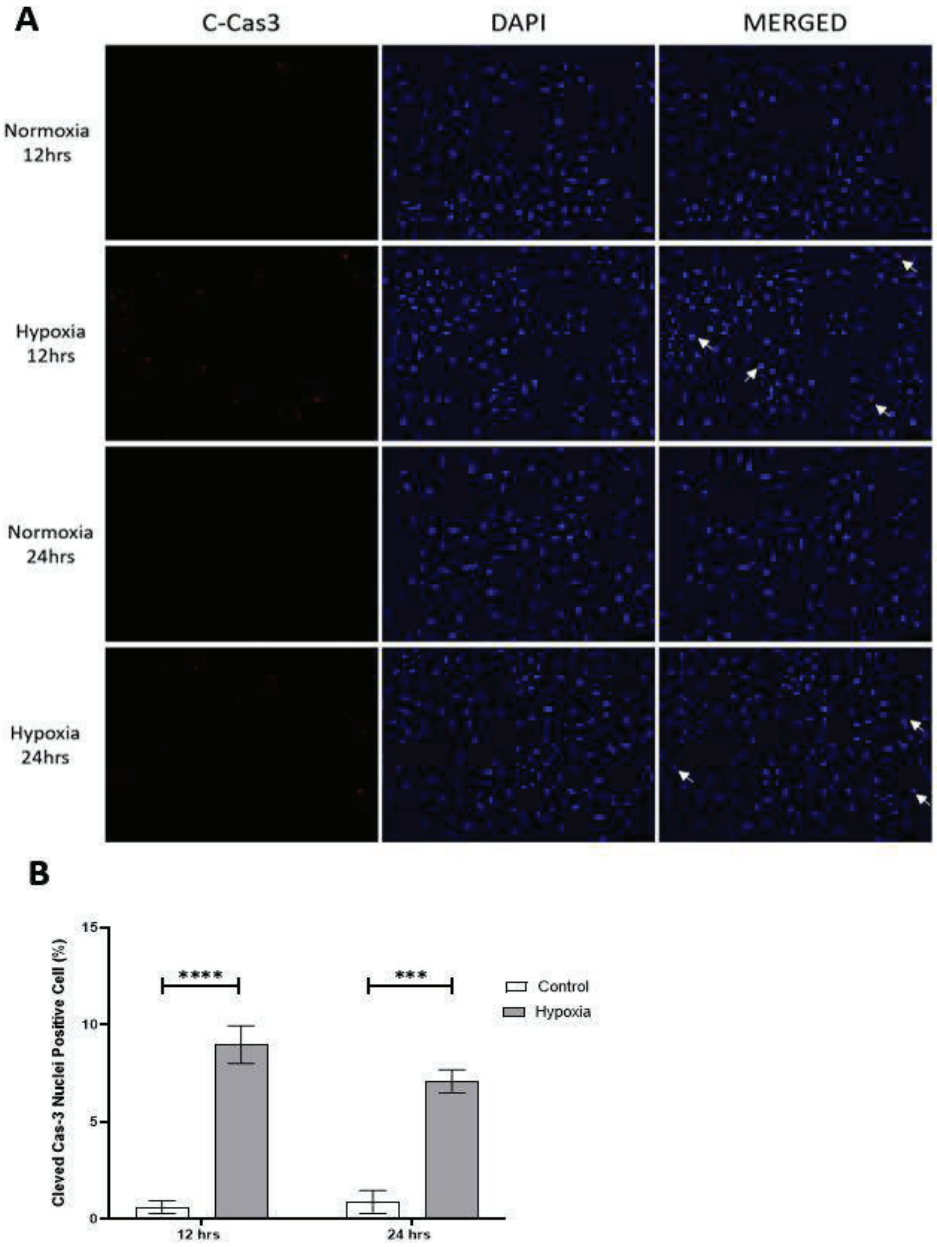

Figure 3.26. Cleaved caspase-3 (c-Cas3) activation observed by immunostaining after the hypoxic condition for 12 and 24-hour.

A. Representative c-Cas3, DAPI and merged images are from normoxia and hypoxia for 12 and 24-hour.

B. Quantitative analysis of the immunostaining of c-Cas3 for 12 and 24-hour.

Results are given as mean ± SEM, n=3

Cleaved caspase-3 translocation to the nucleus was used as apoptotic marker after the cells were exposure to hypoxic environment for 12 and 24-hours with their control group first via immunostaining. All the time-points were stained and their images were captured at the same time. Experiments were conducted in one independent experiment (n=1) and statistical analysis was done using two-way ANOVA and Tukey posthoc analysis. Cleaved caspase-3 was also investigated with Western blotting at 12-hour exposure. Experiments were conducted in three independent experiments (n=3) and statistical analysis was done using two-way ANOVA and Tukey posthoc analysis.

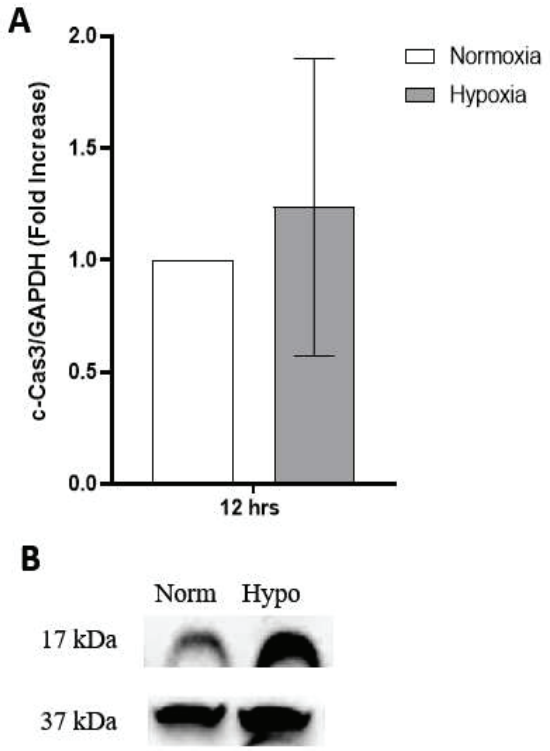

Figure 3.27. Cleaved caspase-3 protein quantified with Western blot after exposure to hypoxic conditions for 12-hour.
A. Quantification analysis of the western blot for c-Cas3 for 12-hour. The data normalized with GAPDH.
B. Expression of c- Cas3 and GAPDH as a loading control for 12-hour with their normoxia and hypoxia group.
(***p<0.001; ****p<0.0001).

Immunostaining revealed that 12 and 24-hour hypoxia caused a significant increase in the number of cleaved caspase-3 positive cells in the nucleus. The quantification of cleaved caspase-3 revealed a 14-fold increase in nuclear translocation at

12-hours after hypoxia induction when compared to normoxic controls. On the other hand, 24-hour hypoxia experiment demonstrated a 7-fold increase when the compared to controls (Figure 3.14).

In addition, cleaved caspase-3 was quantified with Western blot after the cells were exposure to hypoxia at 12-hours. After cleaved caspase-3 was normalized to GAPDH, the results showed the total cleaved caspase-3 expression was a slight increase of 1.2-fold when compared to controls at this time-point (Figure 3.15). However, this difference did not reach significance between groups.

CHAPTER 4

DISCUSSION AND CONCLUSION

HIF is an important transcription factor that plays a crucial role during hypoxia that bind to hypoxia response elements so that cells can adapt to a hypoxic environment. The expression of HIF1 has been extensively reported in CNS injuries that involve hypoxia and ischemia. Following an insult, the resulting of HIF1 expression can act in a biphasic fashion depending on the duration of hypoxia and the specific cell type (Shi 2009; Singh *et al.* 2002). HIF1 could either be neuroprotective or can worsen damage in cells by triggering pro-inflammatory signals or apoptosis. Understanding how different cells react following HIF1 upregulation is important in determining the fate of the cell.

HIF1 can be upregulated *in vitro* with O_2 dependent and independent ways. Cobalt chloride is a chemical inducer of hif1-α that is not dependent on the external O_2 concentration. As a result, hif1-α can translocate into the nucleus and dimerize with Hif1-ß to form the HIF1 transcription factor. On the other hand, O_2 dependent pathways require a reduced amount of oxygen that can be acquired by creating a hypoxic environment. However, hypoxic chambers can be costly for small labs. For this reason, a hypoxia chamber can be assembled in a low-cost and effective way by the use of inflatable plastic bag (Ruoxiang *et al.* 2014). This novel hypoxic chamber has been adopted successfully to trophoblast stem cells (Natale *et al.* 2017), breast cancer cell lines (Khan *et al.* 2018) and dermal fibroblast cell lines (Barlian & Riani 2018). The lack of O_2 causes translocation of Hif1-α from the cytoplasm into the nucleus. In this study, we used this novel hypoxia chamber model, and filled the resealable bag with a 1 % O_2 gas mixture that was balanced with nitrogen. However, it is possible that the plastic bags can be permeable to O_2 to a certain degree (Bastarrachea *et al.* 2011). The bag must be made of proper plastic type, and the ones used in our study were composed of polyethylene and withstand up to 50 C. In future studies, it would be useful to add an O_2 sensors inside the bag to make sure and validate that there is no leakage and that the O_2 concentration is constant.

In this study, bEnd.3 cells were exposed to a hypoxic environment that was created by the novel hypoxia chamber. We were able to quantify Hif1-α upregulation in

this *in vitro* model to confirm that bEnd.3 cells were hypoxic. Moreover, the morphological changes and cell viability were analyzed in a time-dependent manner to understand the extent of injury. For this purpose, cellular viability was determined based on cell circularity, cleaved caspase-3 activity and NF-κB translocation. In the same cell line, we also chemically induced Hif1-α by exposing cells to different concentration of $CoCl_2$ and documented the changes in their cellular morphology and cell viability by trypan blue staining for comparisons.

Hypoxia caused cellular death in endothelial cells both in $CoCl_2$ exposure and hypoxia chamber models *in vitro*. As $CoCl_2$ is well-known cytotoxic molecule, we made sure that the effective dose was adjusted to bEnd.3 cells with minimum cytotoxicity (100-150 uM). This concentration range was determined based on previous studies from the literature (Muñoz-Sánchez & Chánez-Cárdenas 2018). In these studies, cell viability was document using different assays like 3-(4,5-dimethylthiazol-2-yl)-2,5-diphenyltetrazolium bromide (MTT) or lactose dehydrogenase (LDH) assays in bEnd.3 cells that have been exposed to $CoCl_2$ treatment. Those studies revealed that $CoCl_2$ induced cell death that was enhanced at 24-hour following treatment (Chatard *et al.* 2017). The results presented in our study showed that there was an increasing trend in cell death at both 12 and 24-hour $CoCl_2$ exposure when compared to controls. In addition, the cell death observed with the hypoxia chamber was significantly enhanced at 12-hours compared to normoxic cells. However, no significant change was noted at 24-hours of hypoxia. Other studies have also demonstrated that they were no significant difference in cell death between hypoxic and normoxic experiments at the 24 hour. In those studies, bEn.d3 and HUVEC cells experimented inside growth medium when the cells under hypoxia in traditional hypoxic chamber model (Pichiule *et al.* 2004; Stempien-Otero *et al.* 1999). Our results show that there is a prominent reduction in cell viability at 12 hours when compared to 24-hours of hypoxia. These results could be interpreted as 24-hour hypoxia does not cause cell death in bEnd.3 cell *in vitro* model of hypoxia chamber. However, $CoCl_2$ caused HIF1 upregulation at 24 hours so, it was not able to rescue cellular death. Therefore, it is plausible to think that cellular death could be related with HIF1 expression in bEnd.3 cells.

The cellular morphology is an observable way to identify the cellular integrity, well-being of cells. In microvascular endothelial cells, morphological changes can affect the BBB integrity and permeability. A study by Sun and Wang showed that bEnd.3 cells exposed to oxygen glucose deprivation for 18-hours caused a distinct shape where cell

was less adherent with shrinking cell bodies (Wang *et al.* 2019). In our study, we were able to show a similar change in structure with 100 uM $CoCl_2$ exposure that was noted with a reduction of spindle formation and cells became distinctly round in shape after 12 and 24-hours. On the other hand, cells in the hypoxic chamber for 12 hours showed significantly less spindles extending out of the cells bodies and an overall shrinkage was notable. However, the cellular morphology observed at 24-hours of hypoxia was not as drastic as it was in 12-hours. In parallel to these observations, cell circularity analysis demonstrated that circular cells were more prominent at 12-hours when compared to 24-hours of hypoxic exposure. Cells that have circularity in the range between 0.9-1 indicate that the cells are under stress. Hif1-α expresssion and the cellular morphology relationship has been studied in the literature, specifically in several cancer types. In a mouse tumor model, morphological changes in endothelial cells were detected in Hif1-α deficient mice (Tang *et al.* 2004). For this reason, the expression of HIF1 can effect cellular morphology in the endothelial cells.

When Hif1-α is translocated from the cytoplasm to the nucleus, HIF1 is activated and acts as a transcription factor to transcribe many other hypoxia-related genes. HIF1 is known to transcribe more than 100 genes, which are all related to the cells adaptation to hypoxia. HIF1 is associated with apoptosis in embryonic stem (ES) cells when cells are exposed to hypoxia/ischemia (Carmeliet *et al.* 1998). HIF1 can also be associated with membrane depolarization and mitochondrial malfunction as can be observed during apoptosis (Mellor & Harris 2007). Membrane depolarization has been associated with the newly discovered SUR1/Trpm4 channel in the CNS (Vennekens & Nilius 2007). HIF1 can potentially upregulate this ion channel as there is a Sp1 binding side in promoter region of Abcc8 gene. HIF1 can also regulate the expression of Sp1 since there is a HRE region in the Sp1 promoter region. Sp1 can then upregulate SUR1/Trpm4 channels to regulate cell membrane depolarization. Excessive uncontrolled membrane depolarization followed by an insult to the CNS in microvascular endothelial cells can cause disruption of the BBB integrity that can result in morphological changes causing cellular stress to the endothelial cells. The Hif1-α immunostaining results revealed that the most abundant signal was at 12 hours. Umbilical venous endothelial cells (UVECs) also demonstrated similar results to our observations. The expression of Hif1-α was detected as early as 4-hour after the induction of hypoxia and the peaked at12-hours. The Hif1-α were equalized at 24-hours of hypoxia (Calvani *et al.* 2012). In addition, there was an increasing trend of Hif1-α translocation between 4 to 12-hour of hypoxia. Interestingly, there was no noted

difference in Hif1-α expression at 24 hours between hypoxic and normoxic cells. The detection of Hif1-α translocation into the nucleus could be associated with the observed morphological changes and BBB disruption due to apoptosis in the endothelial cells.

NF-κB is a transcription factor that plays a crucial role in the immune response by regulating inflammation (IL secretion), apoptosis, and cell cycle (Bruning *et al.* 2012). NF-κB is expressed in the cytoplasm under normal conditions and binds to IKB inhibitory proteins. Some inflammatory stimuli like TNF-α and lipopolysachharide (LPS) can phosphorylate the IKK complex that binds NF-κB preventing its translocation into the nucleus. When phosphorylation causes the release of the IKK complex, NF-κB can then be translocated into the nucleus to transcribe target genes (Daniel *et al.* 2015). NF-κB directly upregulates Hif1-α expression under normoxic conditions (Zhang *et al.* 2005) or can regulate Hif1-α stabilization (Balamurugan 20016). Conversely, HIF1 can stimulate NF-κB to activate certain signaling pathways that can shift cells from hypoxic metabolism (Görlach & Bonello 2008). Both mechanisms could be activated by the casein kinase 2 (CK2) to synthesize VEGF following cerebral ischemia (Sarkar *et al.* 2019). However, the HIF1 activated NF-κB pathway has not been completely identified. Further studies are needed to enlighten this pathway. Our results show that NF-κB nuclear translocation occurs at 24-hours after the induction of hypoxia. This translocation was not apparent in other time points observed in this study. Hereby, we can assume that the NF-κB translocation takes place after HIF1 is activated following a hypoxic insult.

Caspase-3 is a protease that plays a role in apoptotic cell death. Activation of caspase-3 takes place according to the cell type or external stimuli detected by these cells. It can also trigger some morphological changes (Alan & Reiner 1999). For this reason, caspase-3 activation has been used as an apoptotic cell death marker. Apoptotic cell death was the mostly commonly identified cell death mechanism in a stroke model of ECs. Apoptosis can be followed by autophagy (Zille *et al.* 2019). It has been reported that the caspase-3 activation occurs in a time-dependent fashion, and is the highest at 12-hours in bEnd.3 cells that have been exposed to oxygen glucose deprivation (Liu et al. 2016). Similar results were also shown in a more recent study in human brain microvascular endothelial cells (HBMEC) (Wu *et al.* 2019). Pigs that were exposed to MCAO for 30 minutes had disruption in their TJs that were associated with caspase-3 activation (Zehendner 2011). Our caspase-3 immunostaining results show that there was a significant difference between normoxic and hypoxic groups for both 12 and 24-hour time points. For this reason, caspase activation can trigger apoptosis in bEnd.3 cells in

our hypoxic chamber model. On the other hand, Western blot results of cleaved caspase 3 were also increased at 12-hours after the induction of hypoxia when compared to controls.

Cellular death was observed in this study with Trypan blue staining. The hypoxia chamber model showed that the cellular death peaks at 12-hours of hypoxia exposure. However, 24-hours of hypoxia did not show any change in cell viability when compared with normoxic cells at this time point. Interestingly, cellular death was significantly reduced at 24-hours when compared to 12-hours of hypoxia. We could assume that even if the apoptotic marker was still elevated at 24-hours, bEnd.3 cells could be rescued. Moreover, cell death at 12-hours can most likely take place in a caspase-3 dependent apoptosis mechanism.

As a result of this study, Hif1-α in bEnd.3 cells could be triggered by the novel hypoxia chamber model. Hif1-α activation is associated with cell death and the activation of the NF-κB signaling pathway. ECs membrane depolarization has been associated with apoptosis. This membrane depolarization can be triggered by the activation of SUR1/Trpm4 channels that can in turn regulate BBB disruption, edema formation, and cell death with the AQP4 channels. NF-κB is also another transcription factor that binds the *Abcc8* promoter that regulates Sur1 transcription activated following hypoxia. It is also known that Hif1-α can upregulate NF-κB (Scortegagna 2008) For this reason, the upregulation of Hif1-α can be considered as an early event in hypoxia that can alter NF-κB activation later on. Activated NF-κB could destroy cellular membrane potential via the upregulated SUR1/TRPM4 channels. However, at the early phase of hypoxia, Hif1-α has the potential to elevate cellular death on its own. For this reason, glibenclamide could potentially be used for future studies to identify the role of SUR1/TRPM4 channels in the regulation of cell death following to hypoxia. On the other hand, in this study we only studied a hypoxic condition (1 % oxygen) with glucose in the cell media. To mimic ischemia, lack of complete glucose in the media could be used to induced OGD in endothelial cells which is expected to exacerbate hypoxic response in cells.

In this study, we also tried a novel hypoxic chamber model to mimic a hypoxic environment for *in vitro* studies. For this reason, cellular death and morphological changes were compared to the chemically induced $CoCl_2$ model. Both methods gave similar results up to 12-hours of hypoxic exposure. After that time point, $CoCl_2$ shows continued increase in cellular death in a dose-dependent manner, but in the hypoxia chamber model cells were rescued. Hif1-α could be a key regulator of this noted

difference because of the reduced damage at 24-hours hypoxia chamber model. $CoCl_2$ directly regulate Hif1-α so HIF1 continue to bind hypoxia related genes to further induce apoptosis. Thus, the hypoxia chamber model could be useful in mimicking a hypoxic environment without the use of a chemical inducer that can be cytotoxic to cells. This model could be modified for further experiments of hypoxia and ischemia in *in vitro* studies.

REFERENCES

Abbott, N., Patabendige, A., Dolman, D., Yusof, S., & Begley, D. (2010). Structure and function of the blood–brain barrier. *Neurobiology Of Disease*, 37(1), 13-25. doi: 10.1016/j.nbd.2009.07.030

Abbott, N., Rönnbäck, L. & Hansson, E. Astrocyte–endothelial interactions at the blood–brain barrier. *Nat Rev Neurosci* 7, 41–53 (2006).

Abdullahi, W., Tripathi, D., & Ronaldson, P. T. (2018). Blood-brain barrier dysfunction in ischemic stroke: targeting tight junctions and transporters for vascular protection. American journal of physiology. *Cell physiology*, 315(3), C343–C356.

Aittoniemi, J., Fotinou, C., Craig, T. J., de Wet, H., Proks, P., & Ashcroft, F. M. (2009). Review. SUR1: a unique ATP-binding cassette protein that functions as an ion channel regulator. *Philosophical transactions of the Royal Society of London. Series B, Biological sciences*, 364(1514), 257–267.

Alquisiras-Burgos, I., Ortiz-Plata, A., Franco-Pérez, J., Millán, A., & Aguilera, P. (2020). Resveratrol reduces cerebral edema through inhibition of de novo SUR1 expression induced after focal ischemia. *Experimental neurology*, 330, 113353.

Armulik, A., Genové, G., Mäe, M. et al. Pericytes regulate the blood–brain barrier. *Nature* 468, 557–561 (2010).

Bae, Y. H., Joo, H., Bae, J., Hyeon, S. J., Her, S., Ko, E., Choi, H. G., Ryu, H., Hur, E. M., Bu, Y., & Lee, B. D. (2018). Brain injury induces HIF-1α-dependent transcriptional activation of LRRK2 that exacerbates brain damage. *Cell death & disease*, 9(11), 1125.

Balamurugan K. (2016). HIF-1 at the crossroads of hypoxia, inflammation, and cancer. *International journal of cancer*, 138(5), 1058–1066.

Baranova, O., Miranda, L. F., Pichiule, P., Dragatsis, I., Johnson, R. S., & Chavez, J. C. (2007). Neuron-specific inactivation of the hypoxia inducible factor 1 alpha increases brain injury in a mouse model of transient focal cerebral ischemia. *The Journal of neuroscience : the official journal of the Society for Neuroscience*, 27(23), 6320–6332.

Barlian, A., & Riani, Y. (2018). Correlation of Hypoxia and Pro-senescence Protein Expression in Green Sea Turtle (Chelonia mydas) Lung Epithelial and Dermal Fibroblast Cell Culture. *Journal Of Mathematical And Fundamental Sciences*, 50(1), 59-71.

Bastarrachea, L., Dhawan, S., & Sablani, S. (2011). Engineering Properties of Polymeric-Based Antimicrobial Films for Food Packaging: A Review. *Food*

Engineering Reviews, 3(2), 79-93. doi: 10.1007/s12393-011-9034-8

Bogdanovski, D., DiFazio, L., Bogdanovski, A., Csóka, B., Jordan, G., & Paul, E. et al. (2017). Hypoxia-inducible-factor-1 in trauma and critical care. *Journal Of Critical Care*, 42, 207-212. doi: 10.1016/j.jcrc.2017.07.029

Bruick RK (2003) Oxygen sensing in the hypoxic response pathway: regulation of the hypoxia-inducible transcription factor. *Genes Dev* 17:2614–2623

Bruning, U., Fitzpatrick, S. F., Frank, T., Birtwistle, M., Taylor, C. T., & Cheong, A. (2012). NFκB and HIF display synergistic behaviour during hypoxic inflammation. *Cellular and molecular life sciences: CMLS*, 69(8), 1319–1329.

Burke, M., Mutharasan, R., & Ardehali, H. (2008). The Sulfonylurea Receptor, an Atypical ATP-Binding Cassette Protein, and Its Regulation of the KATPChannel. *Circulation Research*, 102(2), 164-176. doi: 10.1161/circresaha.107.165324

Cai, Z., Qiao, P. F., Wan, C. Q., Cai, M., Zhou, N. K., & Li, Q. (2018). Role of Blood-Brain Barrier in Alzheimer's Disease. *Journal of Alzheimer's disease : JAD*, 63(4), 1223–1234.

Calvani, M., Comito, G., Giannoni, E., & Chiarugi, P. (2012). Time-dependent stabilization of hypoxia inducible factor-1α by different intracellular sources of reactive oxygen species. *PloS one*, 7(10), e38388.

Carmeliet P, Dor Y, Herbert JM, Fukumura D, Brusselmans K, Dewerchin M, Neeman M, Bono F, Abramovitch R, Maxwell P, Koch CJ, Ratcliffe P, Moons L, Jain RK, Collen D, Keshert E, Keshet E. (1998). Role of HIF-1α in hypoxia-mediated apoptosis, cell proliferation and tumour angiogenesis. *Nature.* ;6692:485–490.

Chatard, M., Puech, C., Perek, N., & Roche, F. (2017). Hydralazine is a Suitable Mimetic Agent of Hypoxia to Study the Impact of Hypoxic Stress on In Vitro Blood-Brain Barrier Model. *Cellular physiology and biochemistry : international journal of experimental cellular physiology, biochemistry, and pharmacology*, 42(4), 1592–1602.

Chen WY, Chang MS (2009) IL-20 is regulated by hypoxia-inducible factor and up-regulated after experimental ischemic stroke. *J Immunol* 182:5003–5012

Chen, C., Hu, Q., Yan, J., Lei, J., Qin, L., Shi, X., Luan, L., Yang, L., Wang, K., Han, J., Nanda, A., & Zhou, C. (2007). Multiple effects of 2ME2 and D609 on the cortical expression of HIF-1alpha and apoptotic genes in a middle cerebral artery occlusion-induced focal ischemia rat model. *Journal of neurochemistry*, 102(6), 1831–1841.

Cheng, Y., Park, J., Manzanero, S., Choi, Y., Baik, S., & Okun, E. et al. (2014). Evidence that collaboration between HIF-1α and Notch-1 promotes neuronal

cell death in ischemic stroke. *Neurobiology Of Disease*, 62, 286-295.

Daneman, R., & Prat, A. (2015). The Blood–Brain Barrier. *Cold Spring Harbor Perspectives In Biology*, 7(1), a020412. doi: 10.1101/cshperspect.a020412

Daniel Bandarra, John Biddlestone, Sharon Mudie, H.-Arno J. Müller, Sonia Rocha. (2015) HIF-1α restricts NF-κB-dependent gene expression to control innate immunity signals. *Dis Model Mech* ; 8 (2): 169–181.

Desai, B. S., Monahan, A. J., Carvey, P. M., & Hendey, B. (2007). Blood-brain barrier pathology in Alzheimer's and Parkinson's disease: implications for drug therapy. *Cell transplantation*, 16(3), 285–299.

Devraj, G., Guérit, S., Seele, J., Spitzer, D., Macas, J., Khel, M. I., Heidemann, R., Braczynski, A. K., Ballhorn, W., Günther, S., Ogunshola, O. O., Mittelbronn, M., Ködel, U., Monoranu, C. M., Plate, K. H.,

Hammerschmidt, S., Nau, R., Devraj, K., & Kempf, V. (2020). HIF-1α is involved in blood-brain barrier dysfunction and paracellular migration of bacteria in pneumococcal meningitis. *Acta neuropathologica*, 140(2), 183–208.

Ding, J. Y., Kreipke, C. W., Speirs, S. L., Schafer, P., Schafer, S., & Rafols, J. A. (2009). Hypoxia-inducible factor-1alpha signaling in aquaporin upregulation after traumatic brain injury. *Neuroscience letters*, 453(1), 68–72.

Gerzanich, V., Kwon, M. S., Woo, S. K., Ivanov, A., & Simard, J. M. (2018). SUR1-TRPM4 channel activation and phasic secretion of MMP-9 induced by tPA in brain endothelial cells. *PloS one*, 13(4), e0195526.

Gerzanich, V., Stokum, J. A., Ivanova, S., Woo, S. K., Tsymbalyuk, O., Sharma, A., Akkentli, F., Imran, Z., Aarabi, B., Sahuquillo, J., & Simard, J. M. (2019). Sulfonylurea Receptor 1, Transient Receptor Potential Cation Channel Subfamily M Member 4, and KIR6.2:Role in Hemorrhagic Progression of Contusion. *Journal of neurotrauma*, 36(7), 1060–1079.

Gerzanich, V., Woo, S. K., Vennekens, R., Tsymbalyuk, O., Ivanova, S., Ivanov, A., Geng, Z., Chen, Z., Nilius, B., Flockerzi, V., Freichel, M., & Simard, J. M. (2009). De novo expression of Trpm4 initiates secondary hemorrhage in spinal cord injury. *Nature medicine*, 15(2), 185–191.

Görlach, A., & Bonello, S. (2008). The cross-talk between NF-kappaB and HIF-1: further evidence for a significant liaison. *The Biochemical journal*, 412(3), e17–e19.

Grover, G. J., & Garlid, K. D. (2000). ATP-Sensitive potassium channels: a review of their cardioprotective pharmacology. *Journal of molecular and cellular cardiology*, 32(4), 677–695.

Hamm, S., Dehouck, B., Kraus, J., Wolburg-Buchholz, K., Wolburg, H., Risau, W., Cecchelli, R., Engelhardt, B., & Dehouck, M. P. (2004). Astrocyte mediated

modulation of blood-brain barrier permeability does not correlate with a loss of tight junction proteins from the cellular contacts. *Cell and tissue research*, 315(2), 157–166.

Hansen, J. (2006). Towards Selective Kir6.2/SUR1 Potassium Channel Openers, Medicinal Chemistry and Therapeutic Perspectives. *Current Medicinal Chemistry*, 13(4), 361-376. doi: 10.2174/092986706775527947

Helton, R., Cui, J., Scheel, J. R., Ellison, J. A., Ames, C., Gibson, C., Blouw, B., Ouyang, L., Dragatsis, I., Zeitlin, S., Johnson, R. S., Lipton, S. A., & Barlow, C. (2005). Brain-specific knock-out of hypoxia-inducible factor-1alpha reduces rather than increases hypoxic-ischemic damage. *The Journal of neuroscience : the official journal of the Society for Neuroscience*, 25(16), 4099–4107.

Jha, R. M., Bell, J., Citerio, G., Hemphill, J. C., Kimberly, W. T., Narayan, R. K., Sahuquillo, J., Sheth, K. N., & Simard, J. M. (2020). Role of Sulfonylurea Receptor 1 and Glibenclamide in Traumatic Brain Injury: A Review of the Evidence. *International journal of molecular sciences*, 21(2), 409.

Jiang, B., Li, L., Chen, Q. et al. Role of Glibenclamide in Brain Injury After Intracerebral Hemorrhage. *Transl. Stroke Res*. 8, 183–193 (2017).

Kadry, H., Noorani, B., & Cucullo, L. (2020). A blood-brain barrier overview on structure, function, impairment, and biomarkers of integrity. *Fluids and barriers of the CNS*, 17(1), 69.

Karsy, M., Brock, A., Guan, J., Taussky, P., Kalani, M. Y., & Park, M. S. (2017). Neuroprotective strategies and the underlying molecular basis of cerebrovascular stroke. *Neurosurgical focus*, 42(4), E3.

Ke, Q., & Costa, M. (2006). Hypoxia-inducible factor-1 (HIF-1). *Molecular pharmacology*, 70(5), 1469–1480. https://doi.org/10.1124/mol.106.027029

Keaney, J., & Campbell, M. (2015). The dynamic blood-brain barrier. *FEBS Journal*, 282(21), 4067-4079. doi: 10.1111/febs.13412

Khan, M., Hwang, J., Seo, Y., Shin, K., Lee, K., & Park, C. et al. (2018). Engineering oxygen nanobubbles for the effective reversal of hypoxia. *Artificial Cells, Nanomedicine, And Biotechnology*, 46(sup3), S318-S327. doi: 10.1080/21691401.2018.1492420

Khanna, A., Walcott, B. P., Kahle, K. T., & Simard, J. M. (2014). Effect of glibenclamide on the prevention of secondary brain injury following ischemic stroke in humans. *Neurosurgical focus,* 36(1), E11.

Kim JY, Ahn HJ, Ryu JH, Suk K, Park JH (2004) BH3-only protein Noxa is a mediator of hypoxic cell death induced by hypoxia-inducible factor 1alpha. *J Exp Med* 199:113–124

Kis, B., Deli, M. A., Kobayashi, H., Abrahám, C. S., Yanagita, T., Kaiya, H., Isse, T., Nishi, R., Gotoh, S., Kangawa, K., Wada, A., Greenwood, J., Niwa, M., Yamashita, H., & Ueta, Y. (2001). Adrenomedullin regulates blood-brain barrier functions in vitro. *Neuroreport*, 12(18), 4139–4142. https://doi.org/10.1097/00001756-200112210-00055

Kunert-Keil, C., Bisping, F., Krüger, J., & Brinkmeier, H. (2006). Tissue-specific expression of TRP channel genes in the mouse and its variation in three different mouse strains. *BMC genomics*, 7, 159.

Langen, U. H., Ayloo, S., & Gu, C. (2019). Development and Cell Biology of the Blood-Brain Barrier. *Annual review of cell and developmental biology*, 35, 591–613.

Lawrence MS, Sun GH, Kunis DM, Saydam TC, Dash R, Ho DY, Sapolsky RM, Steinberg GK. Overexpression of the glucose transporter gene with a herpes simplex viral vector protects striatal neurons against stroke. *J Cereb Blood Flow Metab*. 1996;2:181–185.

Lee, J. H., Cui, H. S., Shin, S. K., Kim, J. M., Kim, S. Y., Lee, J. E., & Koo, B. N. (2013). Effect of propofol post-treatment on blood-brain barrier integrity and cerebral edema after transient cerebral ischemia in rats. *Neurochemical research*, 38(11), 2276–2286.

Lenglet, S., Montecucco, F., and Mach, F. (2015). Role of matrix metalloproteinases in animal models of ischemic stroke. *Curr. Vasc. Pharmacol*. 13, 161–166. doi: 10.2174/15701611113116660161

Li, N., Wu, J. X., Ding, D., Cheng, J., Gao, N., & Chen, L. (2017). Structure of a Pancreatic ATP-Sensitive Potassium Channel. *Cell*, 168(1-2), 101–110.e10.

Liu Y, Cox SR, Morita T, Kourembanas S (1995) Hypoxia regulates vascular endothelial growth factor gene expression in endothelial cells. *Circ Res* 77:638–643

Liu, Y., Jiang, S., Yang, P. Y., Zhang, Y. F., Li, T. J., & Rui, Y. C. (2016). EF1A1/HSC70 Cooperatively Suppress Brain Endothelial Cell Apoptosis via Regulating JNK Activity. *CNS neuroscience & therapeutics*, 22(10), 836–844.

Lochhead, J. J., Yang, J., Ronaldson, P. T., & Davis, T. P. (2020). Structure, Function, and Regulation of the Blood-Brain Barrier Tight Junction in Central Nervous System Disorders. *Frontiers in physiology*, 11, 914.

Makar, T. K., Gerzanich, V., Nimmagadda, V. K., Jain, R., Lam, K., Mubariz, F., Trisler, D., Ivanova, S., Woo, S. K., Kwon, M. S., Bryan, J., Bever, C. T., & Simard, J. M. (2015). Silencing of Abcc8 or inhibition of newly upregulated Sur1-Trpm4 reduce inflammation and disease progression in experimental autoimmune encephalomyelitis. *Journal of neuroinflammation*, 12, 210.

Marchi, N., Granata, T., Ghosh, C., & Janigro, D. (2012). Blood-brain barrier dysfunction and epilepsy: pathophysiologic role and therapeutic approaches. *Epilepsia*, 53(11), 1877–1886.

Marshall, L. F., Smith, R. W., & Shapiro, H. M. (1979). The outcome with aggressive treatment in severe head injuries. Part I: the significance of intracranial pressure monitoring. *Journal of neurosurgery*, 50(1), 20–25.

Martínez-Valverde, T., Vidal-Jorge, M., Martínez-Saez, E., Castro, L., Arikan, F., & Cordero, E. et al. (2015). Sulfonylurea Receptor 1 in Humans with Post-Traumatic Brain Contusions. *Journal Of Neurotrauma*, 32(19), 1478-1487. doi: 10.1089/neu.2014.3706

Mathar, I., Jacobs, G., Kecskes, M., Menigoz, A., Philippaert, K., & Vennekens, R. (2014). TRPM4. *Handbook of experimental pharmacology*, 222, 461–487.

Mehta, R. I., Tosun, C., Ivanova, S., Tsymbalyuk, N., Famakin, B. M., Kwon, M. S., Castellani, R. J., Gerzanich, V., & Simard, J. M. (2015). Sur1-Trpm4 Cation Channel Expression in Human Cerebral Infarcts. *Journal of neuropathology and experimental neurology*, 74(8), 835–849.

Mellor HR, Harris AL. (2007). The role of the hypoxia-inducible BH3-only proteins BNIP3 and BNIP3L in cancer. *Cancer Metastasis Rev.* ;3–4:553–566.

Muñoz-Sánchez, J., & Chánez-Cárdenas, M. (2018). The use of cobalt chloride as a chemical hypoxia model. *Journal Of Applied Toxicology*, 39(4), 556-570. doi: 10.1002/jat.3749

Natale, B., Schweitzer, C., Hughes, M., Globisch, M., Kotadia, R., & Tremblay, E. et al. (2017). Sca-1 identifies a trophoblast population with multipotent potential in the mid-gestation mouse placenta. *Scientific Reports*, 7(1). doi: 10.1038/s41598-017-06008-2

Nichols C. G. (2006). KATP channels as molecular sensors of cellular metabolism. *Nature*, 440(7083), 470–476. https://doi.org/10.1038/nature04711

Nilius, B., Owsianik, G., Voets, T., & Peters, J. A. (2007). Transient receptor potential cation channels in disease. *Physiological reviews*, 87(1), 165–217.

Pichiule, P., Chavez, J., & LaManna, J. (2004). Hypoxic Regulation of Angiopoietin-2 Expression in Endothelial Cells. *Journal Of Biological Chemistry*, 279(13), 12171-12180. doi: 10.1074/jbc.m305146200

Piret, J. P., Mottet, D., Raes, M., & Michiels, C. (2002). Is HIF-1alpha a pro- or an anti-apoptotic protein?. *Biochemical pharmacology*, 64(5-6), 889–892.

Porter, A. G., & Jänicke, R. U. (1999). Emerging roles of caspase-3 in apoptosis. *Cell death and differentiation*, 6(2), 99–104.

Principalli, M. A., Dupuis, J. P., Moreau, C. J., Vivaudou, M., & Revilloud, J. (2015). Kir6.2 activation by sulfonylurea receptors: a different mechanism of action for SUR1 and SUR2A subunits via the same residues. *Physiological reports*, 3(9), e12533.

Rodríguez, C., Ramos-Araque, M. E., Domínguez-Martínez, M., Sobrino, T., Sánchez-Morán, I., Agulla, J., Delgado-Esteban, M., Gómez-Sánchez, J. C., Bolaños, J. P., Castillo, J., & Almeida, A. (2018). Single-Nucleotide Polymorphism 309T>G in the MDM2 Promoter Determines Functional Outcome After Stroke. *Stroke*, 49(10), 2437–2444.

Ruoxiang, W., Fengshuo, J., & Hua, Z. (2014). A novel experimental hypoxia chamber for cell culture. *Am J Cancer Res* 2014;4(1):53-60

Safe, S., Imanirad, P., Sreevalsan, S., Nair, V., & Jutooru, I. (2014). Transcription factor Sp1, also known as specificity protein 1 as a therapeutic target. *Expert opinion on therapeutic targets*, 18(7), 759–769.

Sarkar, S., Chakraborty, D., Bhowmik, A., & Ghosh, M. K. (2019). Cerebral ischemic stroke: cellular fate and therapeutic opportunities. *Frontiers in bioscience (Landmark edition)*, 24, 435–450.

Sasabe, E., Tatemoto, Y., Li, D., Yamamoto, T., & Osaki, T. (2005). Mechanism of HIF-1alpha-dependent suppression of hypoxia-induced apoptosis in squamous cell carcinoma cells. *Cancer science*, 96(7), 394–402.

Schattling B., Steinbach K., Thies E., Kruse M., Menigoz A., Ufer F., Flockerzi V., Brück W., Pongs O., Vennekens R., et al. TRPM4 cation channel mediates axonal and neuronal degeneration in experimental autoimmune encephalomyelitis and multiple sclerosis. *Nat. Med.* 2012;18:1805–1811. doi: 10.1038/nm.3015.

Schuler M, Green DR (2001) Mechanisms of p53-dependent apoptosis. *Biochem Soc Trans* 29:684–688

Scortegagna, M., Cataisson, C., Martin, R. J., Hicklin, D. J., Schreiber, R. D., Yuspa, S. H. and Arbeit, J. M. (2008) HIF-1α regulates epithelial inflammation by cell autonomous NFκB activation and paracrine stromal remodeling. *Blood* 111, 3343–3354

Semenza G. L. (2007). Hypoxia-inducible factor 1 (HIF-1) pathway. *Science's STKE : signal transduction knowledge environment,* 2007(407), cm8.

Semenza, G. L., Jiang, B. H., Leung, S. W., Passantino, R., Concordet, J. P., Maire, P., & Giallongo, A. (1996). Hypoxia response elements in the aldolase A, enolase 1, and lactate dehydrogenase A gene promoters contain essential binding sites for hypoxia-inducible factor 1. *The Journal of biological chemistry*, 271(51), 32529–32537. https://doi.org/10.1074/jbc.271.51.32529

Shenaq, M., Kassem, H., Peng, C., Schafer, S., Ding, J. Y., Fredrickson, V., Guthikonda, M., Kreipke, C. W., Rafols, J. A., & Ding, Y. (2012). Neuronal damage and functional deficits are ameliorated by inhibition of aquaporin and HIF1α after traumatic brain injury (TBI). *Journal of the neurological sciences*, 323(1-2), 134–140.

Shi H. (2009). Hypoxia inducible factor 1 as a therapeutic target in ischemic stroke. *Current medicinal chemistry*, 16(34), 4593–4600.

Shimizu, K., Lacza, Z., Rajapakse, N., Horiguchi, T., Snipes, J., & Busija, D. W. (2002). MitoK(ATP) opener, diazoxide, reduces neuronal damage after middle cerebral artery occlusion in the rat. *American journal of physiology. Heart and circulatory physiology*, 283(3), H1005–H1011.

Simard, J. M., Chen, M., Tarasov, K. V., Bhatta, S., Ivanova, S., Melnitchenko, L., Tsymbalyuk, N., West, G. A., & Gerzanich, V. (2006). Newly expressed SUR1-regulated NC(Ca-ATP) channel mediates cerebral edema after ischemic stroke. *Nature medicine*, 12(4), 433–440.

Simard, J. M., Geng, Z., Woo, S. K., Ivanova, S., Tosun, C., Melnichenko, L., & Gerzanich, V. (2009). Glibenclamide reduces inflammation, vasogenic edema, and caspase-3 activation after subarachnoid hemorrhage. *Journal of cerebral blood flow and metabolism : official journal of the International Society of Cerebral Blood Flow and Metabolism*, 29(2), 317–330.

Simard, J. M., Kahle, K. T., & Gerzanich, V. (2010). Molecular mechanisms of microvascular failure in central nervous system injury--synergistic roles of NKCC1 and SUR1/TRPM4. *Journal of neurosurgery*, 113(3), 622–629.

Simard, J. M., Tsymbalyuk, O., Ivanov, A., Ivanova, S., Bhatta, S., Geng, Z., Woo, S. K., & Gerzanich, V. (2007). Endothelial sulfonylurea receptor 1-regulated NC Ca-ATP channels mediate progressive hemorrhagic necrosis following spinal cord injury. *The Journal of clinical investigation*, 117(8), 2105–2113. https://doi.org/10.1172/JCI32041

Simard, J. M., Woo, S. K., Schwartzbauer, G. T., & Gerzanich, V. (2012). Sulfonylurea receptor 1 in central nervous system injury: a focused review. *Journal of cerebral blood flow and metabolism: official journal of the International Society of Cerebral Blood Flow and Metabolism*, 32(9), 1699–1717.

Singh, N., Sharma, G., Mishra, V. et al. Hypoxia Inducible Factor-1: Its Potential Role In Cerebral Ischemia. *Cell Mol Neurobiol* 32, 491–507 (2012).

Stempien-Otero, A., Karsan, A., Cornejo, C. J., Xiang, H., Eunson, T., Morrison, R. S., Kay, M., Winn, R., and Harlan, J. (1999) *J. Biol. Chem*. 274, 8039–8045

Stokum, J. A., Kwon, M. S., Woo, S. K., Tsymbalyuk, O., Vennekens, R., Gerzanich, V., & Simard, J. M. (2018). SUR1-TRPM4 and AQP4 form a

heteromultimeric complex that amplifies ion/water osmotic coupling and drives astrocyte swelling. *Glia*, 66(1), 108–125.

Sun, H. S., & Feng, Z. P. (2013). Neuroprotective role of ATP-sensitive potassium channels in cerebral ischemia. *Acta pharmacologica Sinica*, 34(1), 24–32.

Sweeney, M., Zhao, Z., Montagne, A., Nelson, A., & Zlokovic, B. (2019). *Blood-Brain Barrier: From Physiology to Disease and Back. Physiological Reviews*, 99(1), 21-78. doi: 10.1152/physrev.00050.2017

Szeto, V., Chen, N. H., Sun, H. S., & Feng, Z. P. (2018). The role of KATP channels in cerebral ischemic stroke and diabetes. *Acta pharmacologica Sinica*, 39(5), 683–694.

Tang, N., Wang, L., Esko, J., Giordano, F., Huang, Y., & Gerber, H. et al. (2004). Loss of HIF-1α in endothelial cells disrupts a hypoxia-driven VEGF autocrine loop necessary for tumorigenesis. *Cancer Cell*, 6(5), 485-495. doi: 10.1016/j.ccr.2004.09.026

Thompson, E. M., Halvorson, K., & McLendon, R. (2018). Sulfonylurea receptor 1 expression is variable in adult and pediatric brain tumors. *Clinical neuropathology*, 37(5), 221–227.

Thompson, E. M., Pishko, G. L., Muldoon, L. L., & Neuwelt, E. A. (2013). Inhibition of SUR1 decreases the vascular permeability of cerebral metastases. *Neoplasia (New York, N.Y.)*, 15(5), 535–543.

Tonra J. R. (2002). Cerebellar susceptibility to experimental autoimmune encephalomyelitis in SJL/J mice: potential interaction of immunology with vascular anatomy. *Cerebellum (London, England)*, 1(1), 57–68.

Tosun, C., Kurland, D. B., Mehta, R., Castellani, R. J., deJong, J. L., Kwon, M. S., Woo, S. K., Gerzanich, V., & Simard, J. M. (2013). Inhibition of the Sur1-Trpm4 channel reduces neuroinflammation and cognitive impairment in subarachnoid hemorrhage. *Stroke*, 44(12), 3522–3528.

Van Acker, Z. P., Luyckx, E., & Dewilde, S. (2019). Neuroglobin Expression in the Brain: a Story of Tissue Homeostasis Preservation. *Molecular neurobiology*, 56(3), 2101–2122.

Vennekens, R., & Nilius, B. (2007). Insights into TRPM4 function, regulation and physiological role. *Handbook of experimental pharmacology*, (179), 269–285.

Virgintino, D., Errede, M., Robertson, D., Capobianco, C., Girolamo, F., Vimercati, A., Bertossi, M., Roncali, L., (2004). Immunolocalisation of tight junction proteins in the adult and developing human brain. *Histochem. Cell Biol*. 122, 51–59.

W. Zhang, I. Potrovita, V. Tarabin, O. Herrmann, V. Beer, F. Weih et al. (2005).

Neuronal activation of NF-kappaB contributes to cell death in cerebral ischemia. *J Cereb Blood Flow Metab* 25, 30–40 DOI: 10.1038/sj.jcbfm.9600004

Wang, G. L., Jiang, B. H., Rue, E. A., & Semenza, G. L. (1995). Hypoxia-inducible factor 1 is a basic-helix-loop-helix-PAS heterodimer regulated by cellular O2 tension. *Proceedings of the National Academy of Sciences of the United States of America,* 92(12), 5510–5514. https://doi.org/10.1073/pnas.92.12.5510

Wang, K., Jing, Y., Xu, C., Zhao, J., Gong, Q., & Chen, S. (2020). HIF-1α and VEGF Are Involved in Deferoxamine-Ameliorated Traumatic Brain Injury. *The Journal of surgical research*, 246, 419–426.

Wang, S., Sun, Z., Wang, F., Guo, H., Chen, L., & Chai, L. et al. (2019). Shuxuetong injection protects cerebral microvascular endothelial cells against oxygen-glucose deprivation reperfusion. *Neural Regeneration Research*, 14(5), 783. doi: 10.4103/1673-5374.249226

Woo, S. K., Kwon, M. S., Geng, Z., Chen, Z., Ivanov, A., Bhatta, S., Gerzanich, V., & Simard, J. M. (2012). Sequential activation of hypoxia-inducible factor 1 and specificity protein 1 is required for hypoxia-induced transcriptional stimulation of Abcc8. *Journal of cerebral blood flow and metabolism : official journal of the International Society of Cerebral Blood Flow and Metabolism*, 32(3), 525–536.

Woo, S. K., Kwon, M. S., Ivanov, A., Gerzanich, V., & Simard, J. M. (2013). The sulfonylurea receptor 1 (Sur1)-transient receptor potential melastatin 4 (Trpm4) channel. *The Journal of biological chemistry*, 288(5), 3655–3667.

Woo, S. K., Tsymbalyuk, N., Tsymbalyuk, O., Ivanova, S., Gerzanich, V., & Simard, J. M. (2020). SUR1-TRPM4 channels, not KATP, mediate brain swelling following cerebral ischemia. *Neuroscience letters*, 718, 134729.

Wu, C., Zhao, J., Chen, Y., Li, T., Zhu, R., Zhu, B., & Zhang, Y. (2019). Tangeretin protects human brain microvascular endothelial cells against oxygen-glucose deprivation-induced injury. *Journal of cellular biochemistry*, 120(4), 4883–4891.

Wu, Y., Wang, X., Zhou, X., Cheng, B., Li, G., & Bai, B. (2017). Temporal Expression of Apelin/Apelin Receptor in Ischemic Stroke and its Therapeutic Potential. *Frontiers in molecular neuroscience*, 10, 1.

Wu, Z., Zhu, S. Z., Hu, Y. F., Gu, Y., Wang, S. N., Lin, Z. Z., Xie, Z. S., & Pan, S. Y. (2016). Glibenclamide enhances the effects of delayed hypothermia after experimental stroke in rats. *Brain research*, 1643, 113–122. https://doi.org/10.1016/j.brainres.2016.04.067

Xu, Z. M., Yuan, F., Liu, Y. L., Ding, J., & Tian, H. L. (2017). Glibenclamide Attenuates Blood-Brain Barrier Disruption in Adult Mice after Traumatic

Brain Injury. *Journal of neurotrauma*, 34(4), 925–933.

Yan J, Zhou B, Taheri S, Shi H (2011) Differential effects of HIF-1 Inhibition by YC-1 on the overall outcome and blood-brain barrier damage in a rat model of ischemic stroke. *PLoS ONE* 6(11):27798

Yang, Y., Cheng, L., Li, L., Li, H., Li, Y., Jin, W., Chen, C., & Zhang, J. (2019). Relationship between HIF-1α and apoptosis in rats with traumatic brain injury and the influence of traditional Chinese medicine Sanqi. *Saudi journal of biological sciences*, 26(8), 1995–1999.

Yeh SH, Ou LC, Gean PW, Hung JJ, Chang WC (2011) Selective inhibition of early-but not late-expressed HIF-1α is neuroprotective in rats after focal ischemic brain damage. *Brain Pathol* 21(3):249–262

Yeh, S. H., Yang, W. B., Gean, P. W., Hsu, C. Y., Tseng, J. T., Su, T. P., Chang, W. C., & Hung, J. J. (2011). Translational and transcriptional control of Sp1 against ischaemia through a hydrogen peroxide-activated internal ribosomal entry site pathway. *Nucleic acids research*, 39(13), 5412–5423. https://doi.org/10.1093/nar/gkr161

Yu, Q. J., Tao, H., Wang, X., & Li, M. C. (2015). Targeting brain microvascular endothelial cells: a therapeutic approach to neuroprotection against stroke. *Neural regeneration research*, 10(11), 1882–1891.

Zaman, K., Ryu, H., Hall, D., O'Donovan, K., Lin, K. I., Miller, M. P., Marquis, J. C., Baraban, J. M., Semenza, G. L., & Ratan, R. R. (1999). Protection from oxidative stress-induced apoptosis in cortical neuronal cultures by iron chelators is associated with enhanced DNA binding of hypoxia-inducible factor-1 and ATF-1/CREB and increased expression of glycolytic enzymes, p21(waf1/cip1), and erythropoietin. *The Journal of neuroscience : the official journal of the Society for Neuroscience*, 19(22), 9821–9830.

Zehendner, C. M., Librizzi, L., de Curtis, M., Kuhlmann, C. R., & Luhmann, H. J. (2011). Caspase-3 contributes to ZO-1 and Cl-5 tight-junction disruption in rapid anoxic neurovascular unit damage. *PloS one*, 6(2), e16760.

Zhang, C., Wu, H., Zhu, X., Wang, Y., & Guo, J. (2011). Role of transcription factors in neurogenesis after cerebral ischemia. *Reviews in the neurosciences*, 22(4), 457–465.

Zhang, Y., Pan, S., Zheng, X., & Wan, Q. (2016). Cytomembrane ATP-sensitive K+ channels in neurovascular unit targets of ischemic stroke in the recovery period. *Experimental and therapeutic medicine*, 12(2), 1055–1059.

Zhang, Z., Yao, L., Yang, J., Wang, Z., & Du, G. (2018). PI3K/Akt and HIF-1 signaling pathway in hypoxia-ischemia (Review). *Molecular medicine reports*, 18(4), 3547–3554.

Zille, M., Ikhsan, M., Jiang, Y., Lampe, J., Wenzel, J., & Schwaninger, M. (2019).

The impact of endothelial cell death in the brain and its role after stroke: A systematic review. *Cell stress*, 3(11), 330–347.